MICROSTRUCTURE SENSING

FROM AUTONOMOUS PLATFORMS

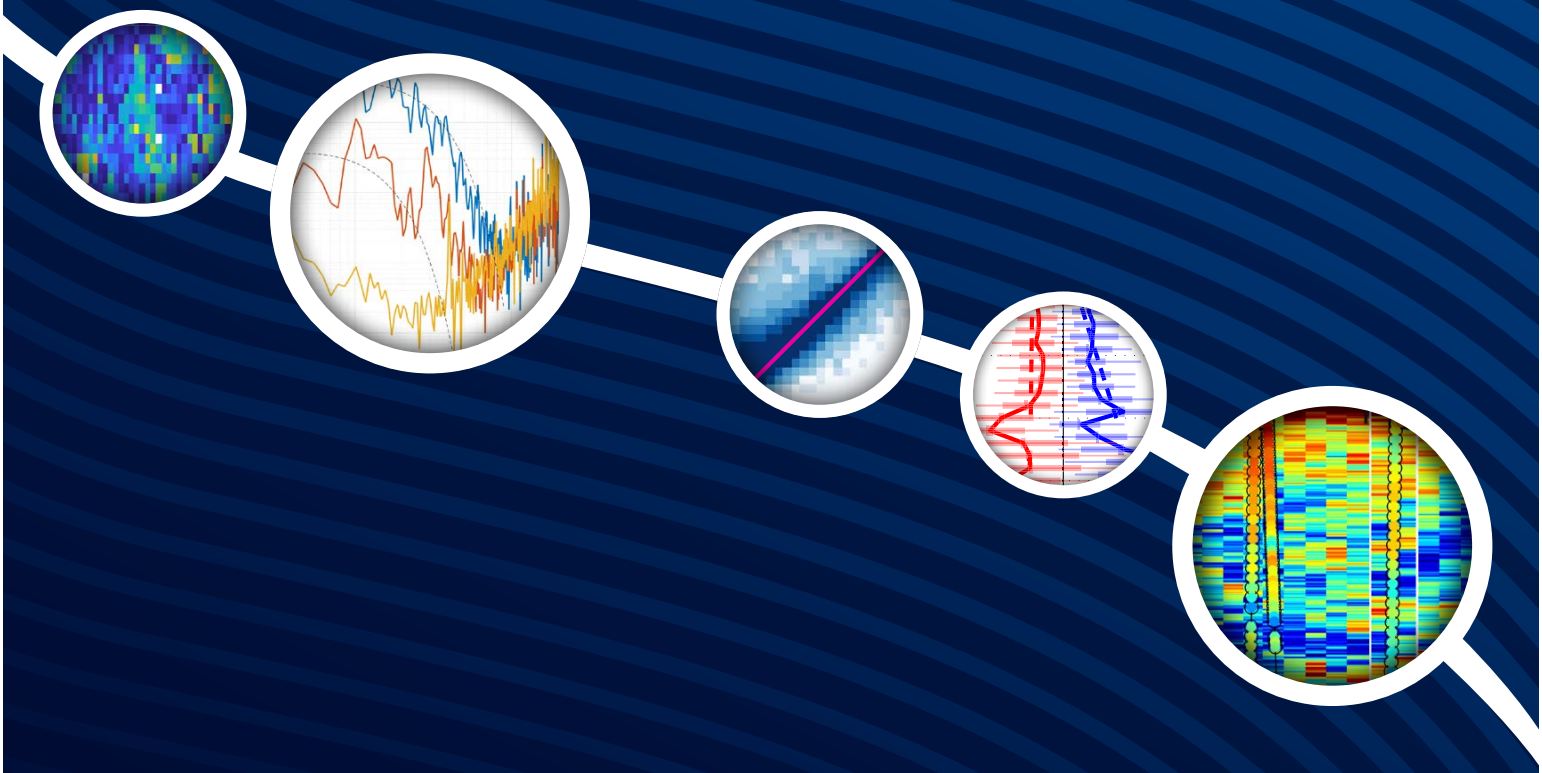

REPORT OF THE OFFICE OF NAVAL RESEARCH SPONSORED WORKSHOP

MAY 2022, LAKE ARROWHEAD, CALIFORNIA

EMILY SHROYER AND LOUIS ST. LAURENT, EDITORS

Acknowledgments

Support for this workshop, report, and the work summarized within was provided by the Office of Naval Research through multiple research grants to individual institutions.

Report Citation

Shroyer, E., and L. St. Laurent, eds. 2023. *Microstructure Sensing from Autonomous Platforms*. Report of the Office of Naval Research Sponsored Workshop, May 2022, Lake Arrowhead, California, 32 pp.

MICROSTRUCTURE SENSING

FROM AUTONOMOUS PLATFORMS

REPORT OF THE OFFICE OF NAVAL RESEARCH SPONSORED WORKSHOP
MAY 2022, LAKE ARROWHEAD, CALIFORNIA

EMILY SHROYER AND LOUIS ST. LAURENT, EDITORS

Contents

In Memory of Lou Goodman

A PIONEER IN AUTONOMOUS SENSING OF TURBULENCE

At the time of this publication, we learned of the passing of Dr. Louis Goodman, who was the Office of Naval Research (ONR) program officer that hosted the 1996 microstructure sensor workshop at Timberline Lodge. Lou served as a program manager at ONR during two terms, from 1978 to 1983, and again from 1993 to 2002. In the time between, he was a research scientist at the Naval Undersea Warfare Center (NUWC) in Newport, Rhode Island, where he conducted influential work on the interaction of turbulent microstructure with high-frequency acoustics (e.g., Goodman, 1990). During his NUWC years he also taught thermodynamics and acoustics as an adjunct professor at the University of Rhode Island, where the coauthor (St. Laurent) became his mentee. Apropos of our workshop topic, Lou worked closely with his NUWC colleague, the late Dr. Ed Levine, to be among the first to equip ocean microstructure sensing on a fully autonomous underwater vehicle (Goodman et al., 2006). Lou finished his career as a professor at the University of Massachusetts - Dartmouth. He became the chair of Department of Ocean and Estuarine Science in 2009 and served in that role until 2012, when he became the associate dean for the School for Marine Science and Technology. In 2013 he became the university's Vice Chancellor for Research and Economic Development and served in that role until he retired in 2015. Lou continued to stay active in research with his colleagues. While his heath issues prevented him from attending the Lake Arrowhead workshop, his influence on the field of microstructure sensing was strongly present.

The two Lous at a meeting in 2017. *Photo Credit: Harper Simmon of APL/UW*

REFERENCES

Goodman, L. 1990. Acoustic scattering from ocean microstructure. *Journal of Geophysical Research: Oceans* 95:11,557–11,573, https://doi.org/10.1029/JC095iC07p11557.

Goodman, L., E. Levine, and R. Lueck. 2006. On closing turbulence budgets from an AUV. *Journal of Atmospheric and Oceanic Technology* 23:977–990, https://doi.org/10.1175/JTECH1889.1.

A photo of the workshop attendees. From left to right: Tom Osborn, Shaun Johnston, Justin Shapiro, Arnaud Le Boyer, Dan Rudnick, Eric D'Asaro, Rolf Lueck, Ken Hughes, Matt Alford, Sophia Merrifield, Steven Jayne, Luc Rainville, Emily Shroyer, Lou St. Laurent, and Fritz Stahr. Missing from the photo: Jim Moum.

Introduction

Emily Shroyer and Louis St. Laurent, Office of Naval Research

Over the last two decades, autonomous sensing of ocean turbulence has progressed from a niche endeavor to one where commercial off-the-shelf hardware is available broadly to the community. This advancement has opened new sampling possibilities, for example, direct observation of turbulence in tropical cyclones, extended observational records much longer than those afforded by ship-based programs, and co-location of multiple platforms for statistical assessment of the natural variation in mixing. The reality of real-time data delivery of turbulence quantities has also introduced challenges for onboard processing, data compression, and quality control of quantities that naturally vary by many magnitudes within short temporal and spatial scales. Developments within autonomous sensing of ocean turbulence continue through advances in software design for efficient and accurate data delivery and hardware design of multiple form factors and sensor combinations.

In 1996, the Office of Naval Research (ONR) held a workshop on microstructure sensors at Timberline Lodge on Mount Hood, Oregon (Agrawal and Williams, 1999). The timing of the workshop was aligned with a paradigm shift in the measurement science of ocean turbulence. The first direct tracer-based, long-term mixing experiments with direct microstructure comparisons were done in a series of experiments by Jim Ledwell and his collaborators (Ledwell et al., 1998). These measurements ended a decades long debate about the validity of diffusivity values being derived from microstructure. Nearly two decades of preceding work had focused on measurements of microstructure in the open-ocean thermocline (Gregg, 1987), generally suggesting that turbulent dissipation rate values beneath the mixed layer were an order of magnitude below the values needed to explain the diffusivity estimate that Munk (1966) derived to describe abyssal stratification. Questions regarding the statistical nature of turbulent events were raised (Gibson, 1982) and dismissed (Davis, 1996). Ultimately, the realization that spatial and temporal variations in ocean physics were key to understanding mixing in the ocean was developing as a major theme.

The first deep measurements of microstructure over rough topography were also made during this time (Polzin et al., 1997). Moreover, the role internal tides play in elevating microstructure signals in areas of rough or steep topography became recognized as an important mechanism (Ledwell et al., 2000). This topic gained momentum in the early 2000s, when large community experiments such as the National Science Foundation-supported Hawaii Ocean Mixing Experiment (Rudnick et al., 2003) and the ONR-supported Nonlinear Internal Wave Initiative

(Tang et al., 2007) were conducted to better understand how the internal wave energy cascade leads to turbulence dissipation and mixing.

The application of autonomous platforms for measuring microstructure is not new. FP07 temperature microstructure probes are the most forgiving sensors for microstructure, as they don't require any specific orientation relative to flow. Their use on early uncrewed underwater vehicle (UUV) systems apparently dates back to the 1970s (Thomas Osborn, Johns Hopkins University, 2022, *pers. comm.*). Profiling floats were likely the first contemporary autonomous system to host FP07 sensors, as pursued by Sherman and Davis (1995). Contemporary navigable UUVs, such as the REMUS and SLOCUM platforms, permit application of airfoil probes designed to measure shear microstructure. Combined temperature, conductivity, and shear microstructure sensing was demonstrated on these systems by Goodman et al. (2006) and Wolk et al. (2009). Microstructure sensing from powered and glider-based propulsion UUVs is now widespread among researchers globally.

The recent proliferation of low-power teraflop-capable embedded processors for the consumer electronics market has provided the resource base for the latest innovation of microstructure sensing: that being onboard processing capability. As described by several contributors to this collection of short papers, the combination of autonomous platform microstructure sensing and onboard processing will revolutionize the study of ocean mixing.

Measurement of ocean turbulence is not a one-size-fits-all technique; instead, multiple approaches can yield meaningful quantification. The need to adjust the measurement technique to platform characteristics (speed, longevity) and targeted environment (e.g., deep ocean or shallow mixed layer) will yield new advances in knowledge and technology. We look forward to seeing what the next two decades may bring in this area of research.

In May 2022, a small group of US scientists convened a two-day workshop focused on "Microstructure Sensing from Autonomous Platforms" in Lake Arrowhead, California. Workshop attendees were sponsored by ONR for engineering development in this topic area, and, in the spirit of past ONR workshops, the participants shared results and discussed recent innovations. Conversations ranged from a historical perspective of ocean turbulence measurement, to new hardware integration of turbulence sensors with autonomous platforms, to algorithms for onboard processing and real-time data delivery. Participants were tasked with developing short synopses of their presentations—nominally three pages and a few figures—for wider distribution.

We give our thanks and appreciation to the scientists who shared their perspectives during the workshop and within the pages of this compilation, which we hope will be of value to the greater community of researchers interested in this topic.

REFERENCES

Agrawal, Y., and A.J. Williams. 1999. Microstructure sensors. *Journal of Atmospheric and Oceanic Technology* 16:1,465–1,466, https://doi.org/10.1175/1520-0426(1999)016<1465:MSDTDR>2.0.CO;2.

Davis, R.E. 1996. Sampling turbulent dissipation. *Journal of Physical Oceanography* 26:341–358, https://doi.org/10.1175/1520-0485(1996)026<0341:STD>2.0.CO;2.

Gibson, C.H. 1982. Alternative interpretations for microstructure patches in the thermocline. *Journal of Physical Oceanography* 12:374–383, https://doi.org/10.1175/1520-0485(1982)012<0374:AIFMPI>2.0.CO;2.

Goodman, L., E. Levine, and R. Lueck. 2006. On measuring the terms of the turbulent kinetic energy budget from an AUV. *Journal of Atmospheric and Oceanic Technology* 23:977–990, https://doi.org/10.1175/JTECH1889.1.

Ledwell, J.R., A.J. Watson, and C.S. Law. 1998. Mixing of a tracer in the pycnocline. *Journal of Geophysical Research: Oceans* 103(C10):21,499–21,529, https://doi.org/10.1029/98JC01738.

Ledwell, J.R., E.T. Montgomery, K.L. Polzin, L.C. St. Laurent, R.W. Schmitt, and J.M. Toole. 2000. Evidence for enhanced mixing over rough topography in the abyssal ocean. *Nature* 403(6766):179–182, https://doi.org/10.1038/35003164.

Munk, W.H. 1966. Abyssal recipes. *Deep Sea Research and Oceanographic Abstracts* 13(4):707–730, https://doi.org/10.1016/0011-7471(66)90602-4.

Polzin, K.L., J.M. Toole, J.R. Ledwell, and R.W. Schmitt. 1997. Spatial variability of turbulent mixing in the abyssal ocean. *Science* 276:93–96, https://doi.org/10.1126/science.276.5309.93.

Sherman, J.T., and R.E. Davis. 1995. Observations of temperature microstructure in NATRE. *Journal of Physical Oceanography* 25:1,913–1,929, https://doi.org/10.1175/1520-0485(1995)025<1913:OOTMIN>2.0.CO;2.

Rudnick, D.L., T.J. Boyd, R.E. Brainard, G.S. Carter, G.D. Egbert, M.C. Gregg, P.E. Holloway, J.M. Klymak, E. Kunze, C.M. Lee, and others. 2003. From tides to mixing along the Hawaiian ridge. *Science* 301(5631):355–357, https://doi.org/10.1126/science.1085837.

Tang, D., J.N. Moum, J.F. Lynch, P. Abbot, R. Chapman, P.H. Dahl, T.F. Duda, G. Gawarkiewicz, S. Glenn, J.A. Goff, and others. 2007. Shallow Water '06: A joint acoustic propagation/nonlinear internal wave physics experiment. *Oceanography* 20(4):156–167, https://doi.org/10.5670/oceanog.2007.16.

Wolk, F., R.G. Lueck, and L. St. Laurent. 2009. Turbulence measurements from a glider. In: *OCEANS 2009,* Conference held October 26–29, 2009, Biloxi, Mississippi, https://doi.org/10.23919/OCEANS.2009.5422413.

Autonomous Ocean Turbulence Measurements Without Microstructure

Eric A. D'Asaro

Microstructure is not the only way to measure oceanic turbulence and sometimes is not even the best way. A full description of turbulence requires measurements of both its large and its small scales. Microstructure focuses on measuring the small scales; alternatives measure the large and intermediate scales of turbulence including their spatial and temporal scales, and their kinetic and potential energies, and image their structure. Successful approaches have included ADCP velocity spectra, the acceleration of floats and gliders, Thorpe overturning scale measurements, imaging using high resolution temperature or density measurements from rapid profilers or temperature chains, and direct covariance flux measurements from floats. These methods work best in high energy environments such as boundary layers, when the overturning scales of the turbulence are comparable or larger than the meter scales of instruments. Some of these are potentially adaptable to widely used platforms such as Argo floats.

SCALES

Figure 1, left, shows the vertical scales of ocean mixing. Turbulent velocities span a range of scales, from the Kolmogorov, where it is limited by viscosity, to the Ozmidov, where it is limited by stratification. These are shown as a function of kinetic energy dissipation rate ε and stratification N. Temperature and salinity fluctuations extend to smaller scales (not shown). Most of the kinetic and potential energy in the turbulence is at the largest scales; most of the dissipation of this energy occurs at the smallest scales. Between these, energy is transferred from the larger scales to the smaller scales across the inertial subrange (gray in the figure). At small ε, the inertial subrange occupies only a small range of scales, centimeters to tens of centimeters; at large ε it can occupy many decades, from millimeters to tens of meters.

Figure 1, right, shows the vertical size of ocean mixing instrumentation and sensors. Typical autonomous vehicles are a meter or so in size. Using these as a traditional microstructure profiler yields measurements from about the size of the vehicle, a meter or so, to the resolution of the sensors, roughly a centimeter for shear and a millimeter for temperature gradient. Autonomous vehicles can also carry traditional CTDs and ADCPs, measuring density and velocity, respectively, as well as one or more pressure sensors measuring vehicle depth. Depending on the sensor and platform, these can measure from a resolution of a few centimeters at most to the length of the profile, many, many hundreds of meters. This note focuses on using these non-microstructure sensors to measure turbulence.

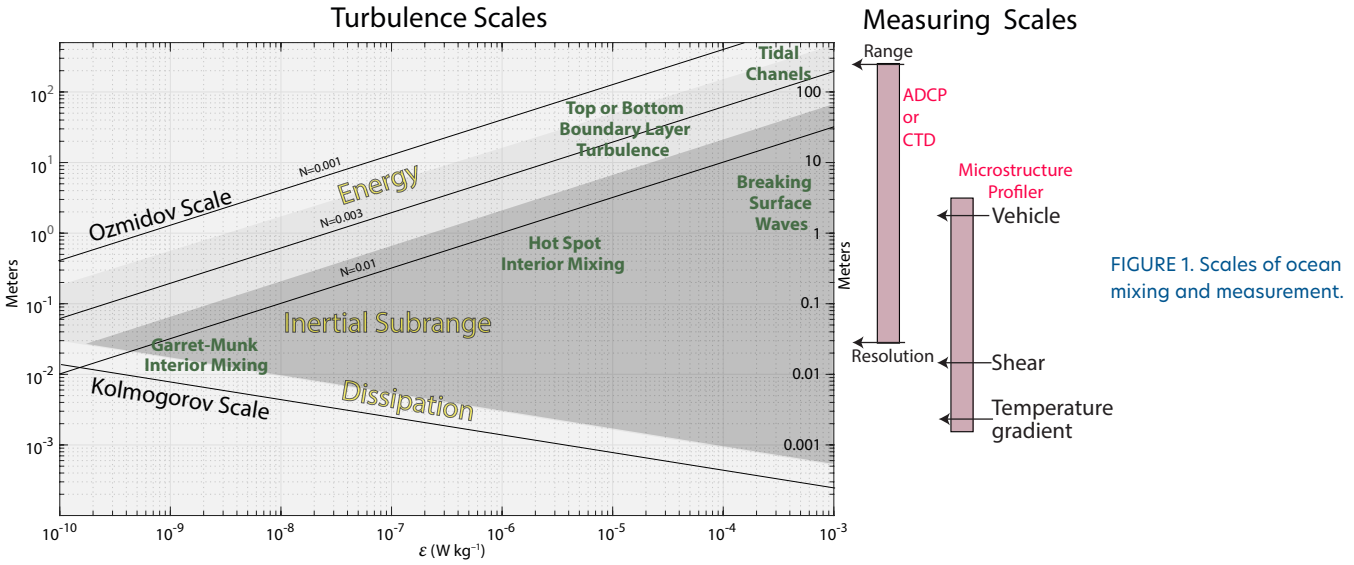

FIGURE 1. Scales of ocean mixing and measurement.

Microstructure methods were developed to measure the very weak and intermittent "Garrett-Munk" turbulence in the ocean interior. For these motions, the measurement range of microstructure profiling nicely spans the range of turbulence scales and this is the preferred method of measurement. However, for more energetic turbulence, at "hot spots" of interior mixing or in the top or bottom boundary layers, the range of turbulence scales becomes much wider, and measurements using other methods become competitive. A few examples are given in this short note.

EXAMPLES

Inertial Subrange Methods

Within the inertial subrange, wavenumber spectra of velocity vary as $\Phi_{uu}(k) = c\varepsilon^{2/3}k^{-5/3}$, where c is a Kolmogorov constant, so that ε can be estimated from the wavenumber spectrum. Similarly, Lagrangian frequency spectra of velocity vary as $\Phi_{uu}(\omega) = \beta\varepsilon\omega^{-2}$ (Lien et al., 1998) so that the spectrum of acceleration is white. For ε larger than about 10^{-8} W kg^{-1}, the scales of the inertial subrange become large enough and the signals strong enough to be measured by inertial subrange methods. Figure 2 shows examples. Thomas et al. (2016) show an example of this method used to address a problem in boundary layer dynamics. Similar approaches have been attempted using gliders (Evans et al., 2018) and density variance dissipation (D'Asaro and Lien, 2007).

Imaging and Thorpe methods

The energetics of stratified mixing can often be addressed by measuring density overturns (Thorpe, 1977) as long as the overturns are large enough to be measured. Figure 3 shows an example using a Lagrangian float that straddled the transition layer at the base of the mixed layer near Ocean Weather Station P during the fall of 2018. The resulting images of the overturning show both infrequent large overturns and many small overturns. An energetic analysis of these indicates that the small overturns are responsible for the turbulent heat flux that deepens the mixed layer.

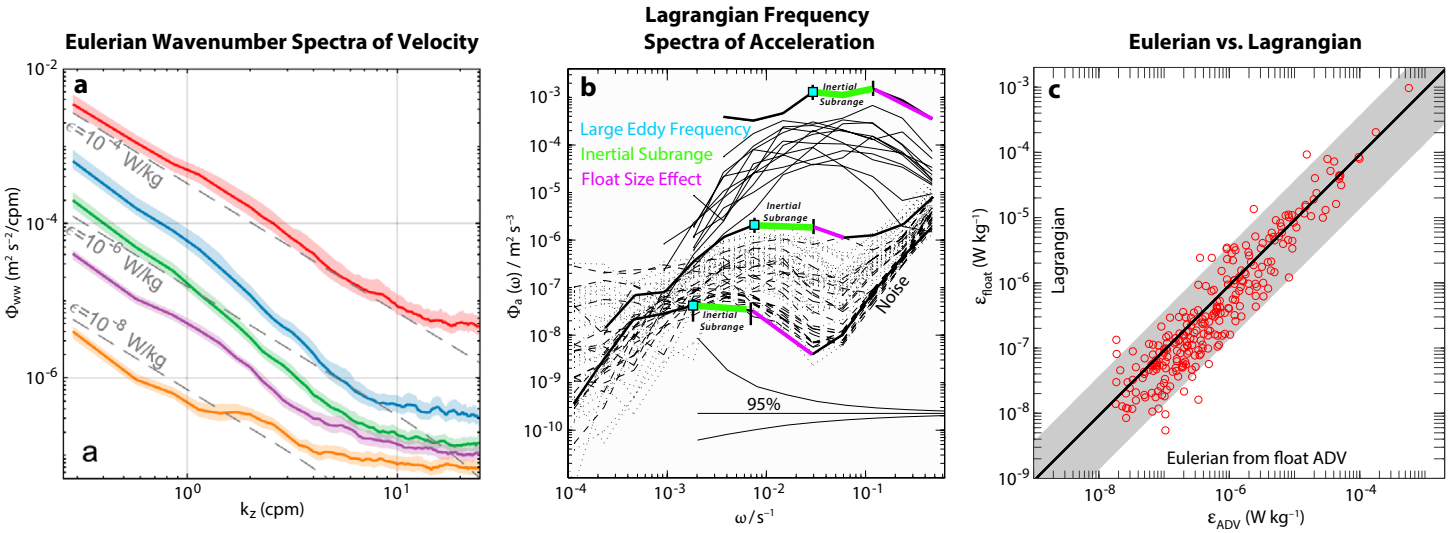

FIGURE 2. (a) Example of Eulerian inertial subranges measured by a Nortek 1000 ADCP operating in HR pulse-pulse mode (Shcherbina et al., 2018). (b) Example of Lagrangian inertial subranges measured from the vertical acceleration of Lagrangian floats measured by pressure (Lien et al., 1998). (c) Comparison of Eulerian and Lagrangian inertial subrange measurements on the same float (Lien and D'Asaro, 2006)

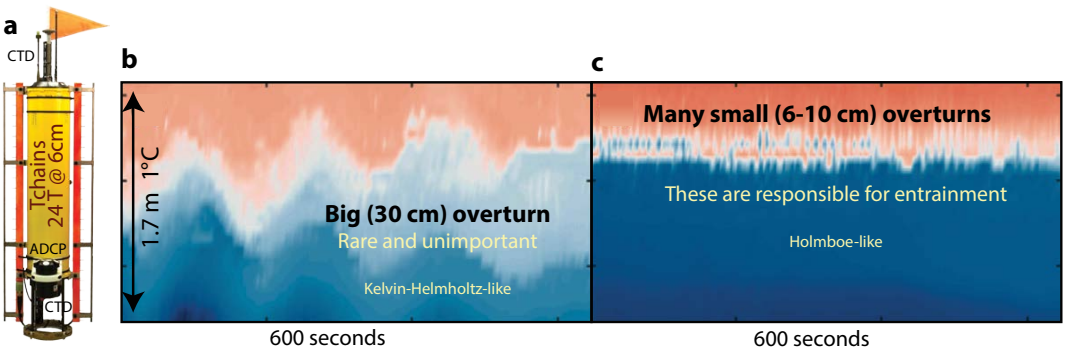

FIGURE 3. (a) A Lagrangian float with two 24-element temperature chains with 6 cm resolution. (b) A Kelvin-Helmholz-like instability in the mixed layer base. (c) Many Holmboe-like instabilities. *Modified from Kaminski et al. (2021)*

Direct Flux Measurement

Covariance fluxes, a centerpiece of turbulence theory, are rarely measured in the ocean because of the difficulty of measuring turbulent vertical velocity in the presence of strong surface and internal wave signals. Figure 4 shows an example of a successful autonomous measurement in the ocean surface boundary layer beneath a hurricane (D'Asaro, 2003).

THE FUTURE

Some of the methods described above may be applicable to Argo floats with only minor modifications. If the upward profiling speed of the floats were reduced, either by software or by adding drag, the existing CTD sensor would have enough resolution to measure the vertical velocity changes and overturning scales of energetic turbulence, either in boundary layers or in hot spots near topography. These methods might also be added to existing autonomous microstructure profiles to augment information on the larger scales. The simple additional of high resolution, internally logging ADCPs to nearly standard profiling floats seems like a particularly promising approach.

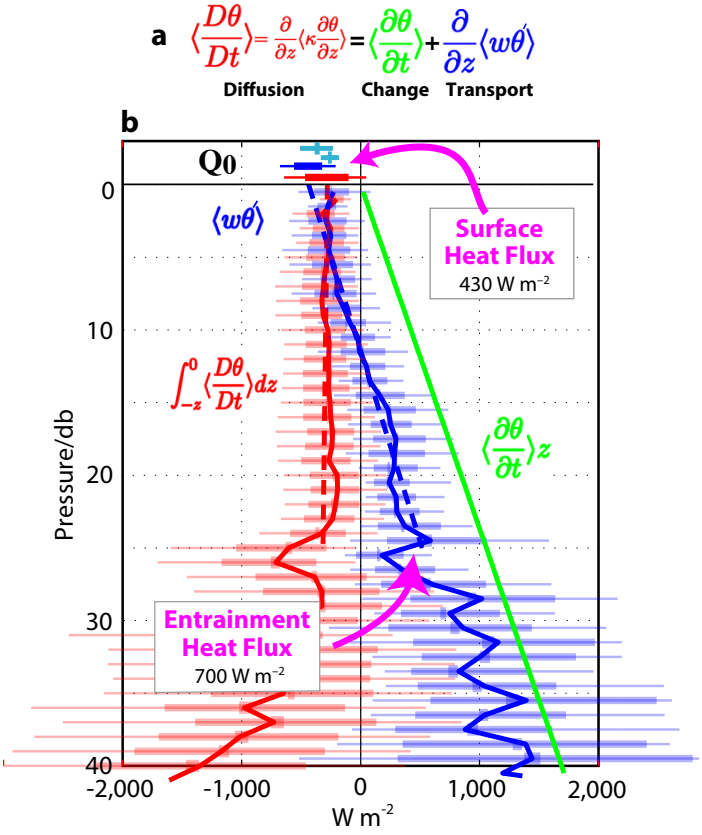

FIGURE 4. (a) The 1D heat equation written in Lagrangian and Eulerian forms (D'Asaro, 2003). (b) Evaluation for a Lagrangian float deployed in Hurricane Dennis shows no parcel heating in the interior (red) consistent with a 1D balance, net cooling of the mixed layer (green) due to the gradient of the vertical heat flux (blue) resulting from surface cooling air-sea fluxes and entrainment cooling at the transition layer.

REFERENCES

D'Asaro, E.A. 2003. The ocean boundary layer below Hurricane Dennis. *Journal of Physical Oceanography* 33(3):561–579, https://doi.org/10.1175/1520-0485(2003)033<0561:TOBLBH>2.0.CO;2.

D'Asaro, E.A., and R.-C. Lien. 2007. Measurement of scalar variance dissipation from Lagrangian floats. *Journal of Atmospheric and Oceanic Technology* 24(6):1,066–1,077, https://doi.org/10.1175/JTECH2031.1.

Evans, D.G., N.S. Lucas, V. Hemsley, E. Frajka-Williams, A.C. Naveira Garabato, A. Martin, S.C. Painter, M.E. Inall, and M.R. Palmer. 2018. Annual cycle of turbulent dissipation estimated from Seagliders. *Geophysical Research Letters* 45(19):10,560–10,569, https://doi.org/10.1029/2018GL079966.

Kaminski, A.K., E.A. D'Asaro, A.Y. Shcherbina, and R.R. Harcourt. 2021. High resolution observations of the North Pacific transition layer from a Lagrangian float. *Journal of Physical Oceanography* 51(10):3,163–3,181, https://doi.org/10.31223/X5J60F.

Lien, R.-C., and E.A. D'Asaro. 2006. Measurement of turbulent kinetic energy dissipation rate with a Lagrangian float. *Journal of Atmospheric and Oceanic Technology* 23(7):964–976, https://doi.org/10.1175/JTECH1890.1.

Lien, R.-C., E.A. D'Asaro, and G.T. Dairiki. 1998. Lagrangian frequency spectra of vertical velocity and vorticity in high-Reynolds-number oceanic turbulence. *Journal of Fluid Mechanics* 362:177–198, https://doi.org/10.1017/S0022112098008787.

Shcherbina, A.Y., E.A. D'Asaro, and S. Nylund. 2018. Observing finescale oceanic velocity structure with an autonomous nortek acoustic Doppler current profiler. *Journal of Atmospheric and Oceanic Technology* 35(2):411–427, https://doi.org/10.1175/JTECH-D-17-0108.1.

Thomas, L.N., J.R. Taylor, E.A. D'Asaro, C.M. Lee, J.M. Klymak, and A. Shcherbina. 2016. Symmetric instability, inertial oscillations, and turbulence at the gulf stream front. *Journal of Physical Oceanography* 46(1):197–217, https://doi.org/10.1175/JPO-D-15-0008.1.

Thorpe, S.A. 1977. Turbulence and mixing in a Scottish loch. *Philosophical Transactions of the Royal Society of London A* 286(1334):125–181, https://doi.org/10.1098/rsta.1977.0112.

AUTHOR

Eric A D'Asaro (dasaro@apl.uw.edu), Applied Physics Laboratory, and School of Oceanography, University of Washington, Seattle, WA, USA.

Different Approaches to Onboard Reduction of Turbulence Data: Pros and Cons

Kenneth G. Hughes and James N. Moum

Many next generation ocean floats and gliders will include turbulence sensors (shear probes and fast thermistors). The way in which we process raw data from these sensors is an active area of research. In particular, it is an open question as to which processing and quality control tasks should be automated and undertaken onboard the instrument prior to satellite transmission and which tasks are better deferred until post-processing and hence undertaken with the oversight of a scientist.

Oceanic turbulence measurements are too data intensive to be transmitted in raw form via satellite. Hence, for turbulence instruments to be expendable or provide near-real-time output, raw data must be reduced in a suitable way. However, there is not one definitive way to do this; to our knowledge, three distinct but overlapping approaches are currently in use or under development. Each approach has its own pros and cons.

Perhaps the most obvious approach is a direct port of a standard turbulence processing routine. For example, take a suite of proven MATLAB code, rewrite it in C, and compile it for an onboard processor. Then, during an experiment, send back profiles of the two most relevant quantities: turbulent dissipation of kinetic energy ε and turbulent dissipation of thermal variance χ. This is certainly an efficient way to compress the data prior to transmission. Even if additional ocean quantities and quality control metrics are also transmitted, the final data set will be small.

Although such a port is possible, it is far from straightforward. First, it is best undertaken by those with working knowledge of *both* the relevant science and engineering (i.e., oceanic turbulence and firmware programming). Second, it introduces many opportunities for errors to creep in. For example, even a high-level description of how to calculate χ for a given segment involves an elaborate sequence of steps. First, calculate ε. This involves calibrating the raw shear probe voltage signal, calculating a frequency spectrum from the calibrated data, converting to a wavenumber spectrum using the measured profiling speed, correcting the spectrum for spatial smoothing by the shear probe, and then iteratively fitting the spectrum to an analytical model spectrum over a variable wavenumber band. Once ε has been found, similar steps are applied to the raw thermistor data. Now consider the effect of an incorrect shear calibration because of some inadvertent mistake (say, the wrong shear probe is installed or the wrong header file is applied). This calibration error causes ε to be wrong, which then causes χ to be wrong as well. Given how the inadvertent error cascades through the algorithm—and the nonlinearity inherent in many of the steps—the two turbulence quantities are

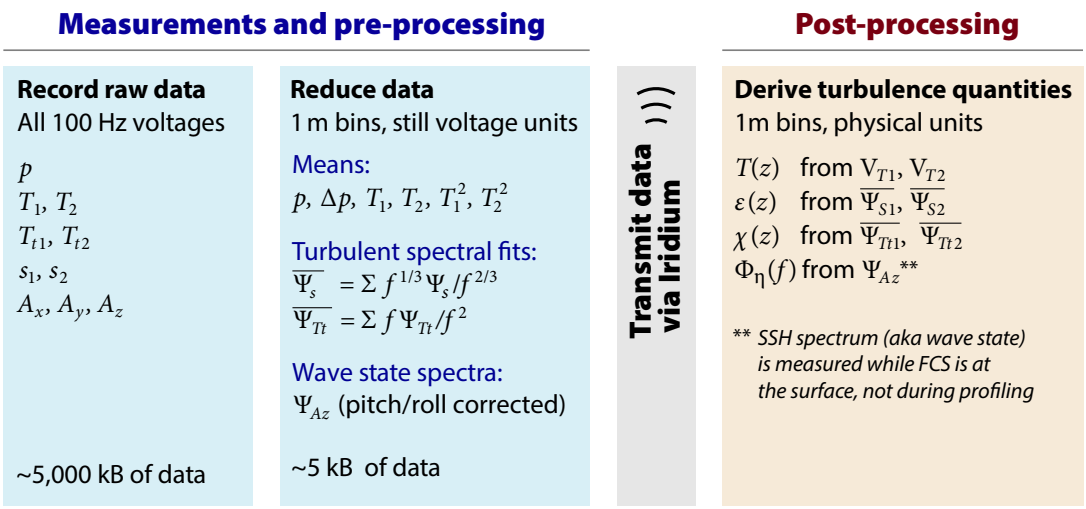

FIGURE 1. The outline of a new turbulence data reduction scheme. See Hughes et al. (2023) for full details.

wrong by amounts that are difficult or impossible to ascertain and fix after the fact.

A second approach, which has been used by Rainville et al. (2017), delays the calibration and fitting until post-processing. Specifically, spectra of shear probe and fast thermistor signals are calculated in voltage units and band-averaged down to, say, 12 values per spectrum. This approach is more data intensive than the prior one, but overcomes its downsides. First, it better separates the scientific and engineering components. That is, the engineer's responsibilities end after having written the software to calculate voltage spectra. The scientist is then responsible for all spectral fitting, quality control, and interpretation. Second, because the onboard component of the routine is simpler, there is less room for error.

Our approach (Hughes et al., 2023), which was primarily developed for Flippin' χSOLO (Moum et al., 2023), shares aspects of the previous two. Like Rainville et al. (2017), we calculate voltage spectra and delay calibration until post-processing. Unlike Rainville et al., we compress each spectrum in terms of a fit metric so as to efficiently compress the data set before transmission.

One unique aspect of our approach is the simple method we use to fit voltage spectra onboard. For shear spectra, we fit to $f^{1/3}$ curves; for thermistor spectra, we fit to f^{1} curves (**Figure 1**). The simplicity of these analytical forms[1] means that the fit metric for each spectrum is calculated with what is effectively a weighted average of the voltage spectrum over a fixed frequency range. Implementing such a fit is straightforward compared to the iterative fits noted earlier, but it does come with a limitation.

Conventional routines use variable wavenumber bands for fitting so as to make use of as much bandwidth of a spectrum as possible. For weak turbulence, much of the spectra is dominated by noise, so a comparatively small band of the spectrum is fit. For strong turbulence, noise is less of an issue and a larger band can be fit. Because our approach uses a fixed frequency range, we must compromise. For the scientific goals of FχS, we are most interested in the larger values of ε. We therefore use a comparatively large upper frequency bound and accept that this introduces a slightly higher noise floor (**Figure 2**).

Each turbulence platform has a niche; there is no one-size-fits-all. The same is true of the data reduction approaches, and we expect all three of the approaches outlined above to thrive. Indeed, that these parallel efforts exist points to the timeliness of the problem and alludes to a shift in how turbulence will be measured in future field campaigns.

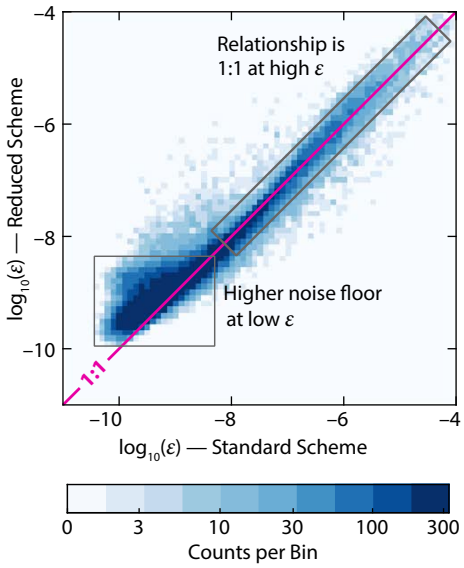

FIGURE 2. Turbulent dissipation ε as calculated by the Hughes et al. (2023) reduction scheme generally agrees well with that from the standard scheme. The one exception is low values of ε where there is a systematic bias: ε from the reduced scheme effectively has a higher noise floor. This two-dimensional histogram comprises 77,000 values.

To our knowledge, few (if any) turbulence instruments have yet been treated as truly expendable, but this will change in the next two years. Expendable profilers will become a necessity as we move away from repeat profiling with one instrument and toward multiple autonomous turbulence floats deployed at once. Onboard turbulence data reduction is helping facilitate this shift.

REFERENCES

Hughes, K.G., J.N. Moum, and D.L. Rudnick. 2023. A turbulence data reduction scheme for autonomous and expendable profiling floats. *Ocean Science* 19(1), https://doi.org/10.5194/os-19-193-2023.

Moum, J.N., K.G. Hughes, D.L. Rudnick, and E.L. Shroyer. 2023. Sampling test of ε featuring Flippin' χSOLO. Pp. 22–23 in *Microstructure Sensing from Autonomous Platforms*. Report of the Office of Naval Research Sponsored Workshop, E. Shroyer and L. St. Laurent, eds., May 2022, Lake Arrowhead, California.

Rainville, L., J.I. Gobat, C. Lee, and G. Shilling. 2017. Multi-month dissipation estimates using microstructure from autonomous underwater gliders. *Oceanography* 30(2):49–50, https://doi.org/10.5670/oceanog.2017.219.

AUTHORS

Kenneth G. Hughes (kenneth.hughes@oregonstate.edu) and **James N. Moum**, both at Oregon State University, Corvallis, OR, USA.

[1] The $f^{1/3}$ and f^{1} curves are low-wavenumber approximations to the Nasmyth and Kraichnan model spectra, respectively. Our paper includes the derivation of functions that correct for these approximations in post-processing.

Attitude of the Flippin' χSOLO

T.M. Shaun Johnston, Daniel L. Rudnick, Benjamin D. Reineman, Kyle Grindley, Michael McClune, Jeffrey Sherman, James N. Moum, Emily L. Shroyer, Kenneth G. Hughes, Pavan Vutukur, Craig Van Appledorn, Kerry Latham, and Aurélie J. Moulin

The Flippin' χSOLO (FχS) provides clean flow and a smooth ride for turbulence sensors by positioning the sensors and the antenna at opposite ends of the float. FχS flips at the bottom/top of each profile to position the sensors into clean flow for ascents/descents at up to 30/20 cm s^{-1}. After flipping, the root mean squared (rms) fluctuation of roll is <1° and the rms fluctuation of vertical profiling speed is 2–4 mm s^{-1}. Other low-power, neutrally buoyant sensors in their own pressure cases can be accommodated in a straightforward fashion. This platform offers a consistent ride for comparing different turbulence sensors. We contemplate some uses for an array of 100 FχS in process studies.

INTRODUCTION

We have designed and built a profiling float, the Flippin' χSOLO (FχS), that supports sensors that require clean flow by moving the sensors and antenna to opposite ends of the float (Figure 1; Moum et al., 2022). The FχS is a modified version of the SOLO-II float and its predecessor, the SOLO float (Davis et al., 2001). SOLO-II floats are currently used in the Argo program and provide a proven, consistently smooth ride. Because the antenna and sensors are at opposite ends of the FχS, the key design feature is the flipping. The platform flips upon arriving at the surface to transmit data with the antenna on the tail out of the water and to position the sensors for the descent (Figure 1). The float flips at the bottom of the profile to position the nose upward for the ascent with the sensors in clean flow. The flip is implemented by shifting the battery pack and obtaining a torque due to the height difference between the centers of gravity and buoyancy.

The FχS combines (a) a turbulence pod with shear probes, thermistors, and accelerometers, and (b) a pumped Sea-Bird glider payload CTD. FχS is designed for an endurance of about 60 days while profiling continuously from the surface to 200 m roughly every 45 minutes, with a typical vertical velocity of 20 cm s^{-1}. A total of about 4,000 profiles are planned, including up- and downcasts. FχS floats return efficiently reduced turbulence data, obviating the need for recovery (Hughes et al., 2023). The float supports any sensor that is small enough to fit on the nose with a diameter of 17 cm, is contained within its own pressure case, is within 200 g of neutral buoyancy, and has power requirements

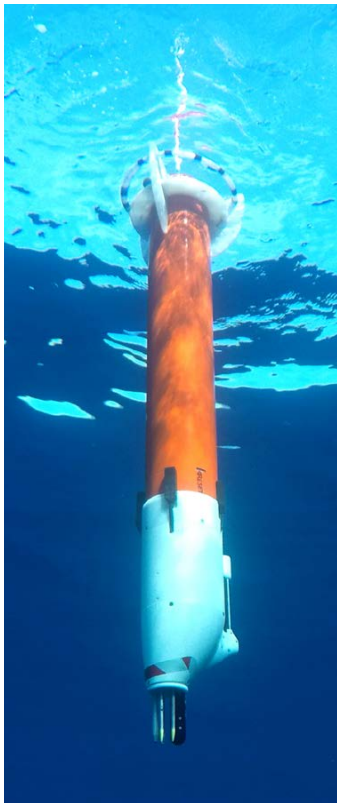

FIGURE 1. FχS is flipped, ready to communicate with the antenna pointed up, and ready to descend with the sensors pointed down into the clean flow during a test off San Diego.

of about 0.4 W. The allocation of battery power can be changed; currently, FχS has 1600 Wh of energy for the platform and 400 Wh for the turbulence pod. The total oil volume available for buoyancy changes is 420 ml, which allows for buoyancy changes of ±215 g on ascent/descent. These features make integration of the sensor package and the float platform straightforward.

Two floats (FχS1 and FχS2) were tested off Oregon from R/V *Oceanus* over 3.5 days in May 2019 and compared to a proven instrument, the Chameleon microstructure profiler (Moum et al., 2022). One purpose of this cruise was to obtain data on the platform motion and vibration, which contribute to the noise floor of the turbulence measurements (Moum and Lueck, 1985). To obtain high-quality, low-noise measurements of turbulence, we minimize vibrations from both platform motion and operation of pumps (for the oil bladder, which provides buoyancy and for the CTD, which provides quality data). The CTD was pumped on descents, but the pump was shut down on ascents for comparisons. FχS1 profiled continuously, while FχS2 was recovered on May 15 for sensor replacement and then deployed again. Median values of turbulence (χ) are at lower levels for FχS1 than FχS2, which suggests a lower noise floor due to weaker levels of vibration for FχS1 (Moum et al., 2022). In both cases, the noise levels of the turbulence measurements are no greater than those from Chameleon.

In the following sections, we describe the vertical velocity and attitude (i.e., roll, pitch, and heading) of the FχS. We obtain our measurements from the accelerometers and compass in the turbulence pod, measure the vertical velocity of the platform, and analyze its attitude. We summarize our findings about the platform's smooth and consistent ride and suggest future uses for an array of 100 floats.

METHODS

Our focus is on data from the Honeywell HMC6343 three-axis linear accelerometer and compass in the turbulence pod, which return data at 4 Hz. The accelerometer is mounted with one axis parallel to the longitudinal axis of the float (i.e., usually vertical), while the other two axes are transverse (i.e., usually horizontal). Heading is a rotation about the vertical axis and is measured by the compass with an arbitrary zero. Tilt is an angle from the vertical, which may be either pitch (with the convention of +90° is nose/sensors up and -90° is nose down) or roll (a tilt about the other horizontal axis which is near 0°). For tilts from the vertical (i.e., in the direction of the gravitational acceleration), these angles are derived from the accelerometers, which have a cosine response for the vertical axis and a sine response for the horizontal axes. The compass is specified with accuracies for heading of 2° rms. The accelerometer is specified with accuracies for tilts from the vertical of ±1° rms. We use pitch mainly to indicate the upward or downward orientation of the float. Variability of pitch and roll are similar (i.e., their rms fluctuations; figure not shown) because they are axisymmetric about the longitudinal axis of the float. We use roll as our principal measure of tilt.

VERTICAL VELOCITY

A profile to 150 m comprises the steady descent (10 min to 130 m), flipping the sensors up (7 min, some of which is spent ascending), the steady ascent (6 min from 120 m), and the flip at the surface to transmit data and position the sensors downward for the next descent (Figure 2). At the surface, the oil moves from the external bladder into the pressure case to begin the descent, while at about 130 m the oil is pumped into the external bladder to stop the descent and provide buoyancy for the ascent. For this contribution, we focus on characterizing the platform motion during the steady ascent/descent.

Vertical ascent/descent speed (w) is obtained by subtracting the standard atmospheric pressure from the 4 Hz pressure data, converting the results to depth, forward differencing, and then smoothing over 5 s (Figure 2a,b). The latter step is

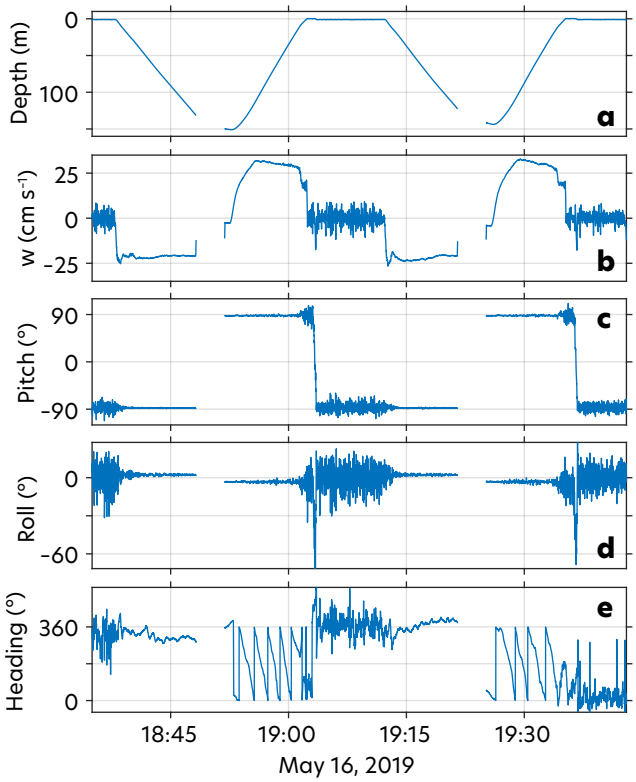

FIGURE 2. Two ascents and descents from FχS1 plotted as a time series show (a) depth, (b) vertical velocity with faster ascents, (c) pitch where sensors are down/up at ±90° with minimal variability during ascent and descent, (d) roll with minimal variability during ascent and descent, and (e) heading with rotations only for FχS1 on ascent. Blank spots indicate the start of a new ascent.

equivalent to smoothing over ~1 m in the vertical. The ballasting of the floats aimed to provide similar w on ascents/descents (mean magnitudes for FχS1 are 21/22 cm s^{-1} from 25 m to 75 m, where the profiling speed is roughly constant). On May 15, some lead ballast was removed from FχS2, producing faster ascents with w > 30 cm s^{-1}.

ATTITUDE

The platform provides a smooth ride, as noted by the accelerometer in the turbulence pod. During the steady portion of the ascents/descents, minimal variability is seen in pitch and roll (Figure 2c,d), except at the surface where the accelerations measure surface waves (Moum et al., 2022; Hughes et al., 2023).

Heading is more variable on descents than pitch/roll and shows a slow rotation on ascent for FχS1 (Figure 2e). FχS2 rotates little on both ascents and descents. Rotation will depend on some combination of (a) the alignment of the tail fins, and (b) asymmetric drag on the tail/nose. A least squares fit over depth corresponding to 25%–75% of the maximum depth provides a rotation rate of 2–3° s^{-1} for all of the ascents. Because there are only a few rotations per 100 m, the turbulence measurements are not affected.

Oscillation amplitudes of about 1° in roll are apparent for FχS1 and FχS2 (Figure 3b). The frequency of these oscillation is identified by a spectral analysis. To obtain the spectra, data are selected from the region of steady w from 20 m to 100 m; these data are detrended, a Hanning window is applied, and segments of 256 points (about 18 m in the vertical) are half-overlapped, and then resulting periodograms are averaged. By looking during steady ascents/descents over the depth range 20–100 m (Figure 3a–c), we identify a dominant period at 7–8 s in roll (Figure 3b,d), which corresponds to a wavelength comparable to the ~2 m length of the float. This may be fortuitous, but could be related to a mode of oscillation. These results are typical for both FχS1 and FχS2. The mixed layer was located at about 15 m depth, above which greater variability is found, which may also be due in part to surface waves (Figure 3a–c).

To further understand the changes of attitude, we examine all of the profiles after the changes in ballasting and profiling depth on May 15. The data extended to 150 m and are placed into 8 m bins, where their means and rms deviations from the mean are calculated. The bin means and rms are then averaged for all of the selected profiles to produce a single profile of mean and rms for each of w and roll (Figure 4). The rms of heading was also calculated. This procedure is applied to FχS1 and FχS2 with similar results for times before and after May 15. After flipping at the top and bottom of the profile, w is small and the float takes >20 m to accelerate to a steady profiling speed. At the top and bottom, rms w is the largest, while from 20 m to 120 m in the region of steady profiling rms w = 2–4 mm s^{-1}, rms pitch is <1° (not shown), and rms roll is <1°. For FχS1, 5 we noted

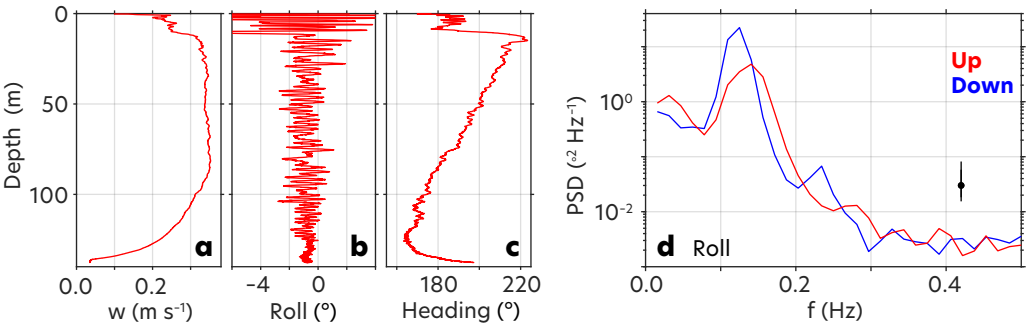

FIGURE 3. On May 17, 2019, at 00:45 from FχS2, the ascending profile of (a) vertical velocity, (b) roll, and (c) heading show steady attitude over the depth range from 20 m to 100 m. (d) Frequency spectra are shown for roll from 20 m to 100 m for both ascent (red) and descent (blue). The 95% confidence interval is shown (black).

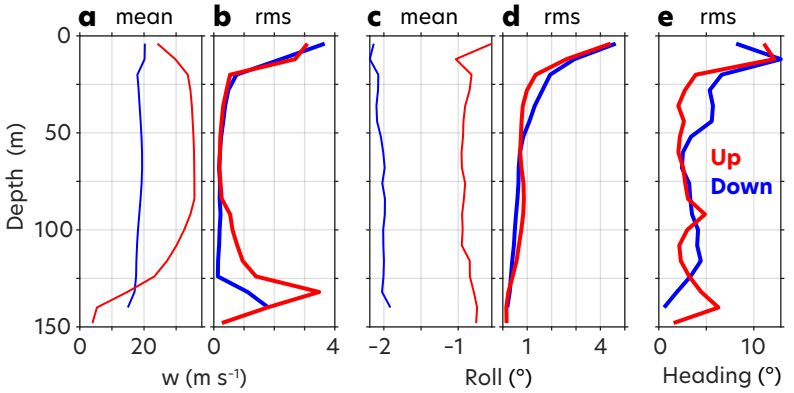

FIGURE 4. For FχS2, profiles of the mean (a) vertical velocity magnitude and (c) roll and rms of (b) vertical velocity, (d) roll, and (f) heading show a region of smooth ascent/descent (red/blue) from about 20 m to 120 m.

a rotation rate of 2°–3° s^{-1} on ascent earlier. FχS2 does not rotate completely and so the rms rotation is less than 5°. After entering the steady portion of the profile, attitude variability is small.

SUMMARY AND DISCUSSION

The FχS provides clean flow and a smooth ride to the turbulence sensors. After flipping, the rms roll is <1° and the rms w is 2–4 mm s^{-1}. Other sensors can be accommodated in a straightforward fashion within the guidelines noted earlier. Thus, this platform offers a consistent ride for comparing different turbulence sensors. Typically a factor of 2 difference is noted in nearby values of turbulent dissipation, which is attributed mainly to variability in geophysical flows (Moum and Lueck, 1985; Moum et al., 2022).

FχS was designed to fill the need for rapidly profiling floats in focused process studies. The intensive observations provided by 100 profiling floats in combination with other assets would be valuable for a process study which simultaneously covered micro-, fine-, submeso-, and mesoscales. Such an array would be a step forward in the examination of (a) the forward cascade of energy at an energetic feature, such as a front (Hoskins and Bretherton, 1972; Rudnick, 2001; Johnston et al., 2011), (b) turbulence measured up to the sea surface under a tropical cyclone (D'Asaro et al., 2011, 2014; Johnston et al., 2020, 2021; Sanabia and Jayne, 2020; Brizuela et al., 2022), or (c) turbulent processes in the equatorial cold tongue, where mixing has a strong effect on air-sea interaction (Moum et al., 2013; Warner and Moum, 2019). Such studies would have wide spatial and temporal coverage, while maintaining the necessary high vertical and horizontal resolution.

REFERENCES

Brizuela, N.G., T.M.S. Johnston, M.H. Alford, O. Asselin, D.L. Rudnick, J.N. Moum, E.J. Thompson, S. Wang, and C.-Y. Lee. 2022. A vorticity-divergence view of internal wave generation by a fast-moving tropical cyclone: Insights from Super Typhoon Mangkhut. *Journal of Geophysical Research: Oceans* 128(5):e2022JC019400, https://doi.org/10.1029/2022JC019400.

D'Asaro, E.A., P.G. Black, L.R. Centurioni, Y.-T. Chang, S.S. Chen, R.C. Foster, H.C. Graber, P. Harr, V. Hormann, R.-C. Lien, and others. 2014. Impact of typhoons on the ocean in the Pacific. *Bulletin of the American Meteorological Society* 95(9):405–418, https://doi.org/10.1175/BAMS-D-12-00104.1.

D'Asaro, E.A., C. Lee, L. Rainville, R. Harcourt, and L. Thomas. 2011. Enhanced turbulence and energy dissipation at ocean fronts. *Science* 332(6027):318–322, https://doi.org/10.1126/science.1201515.

Davis, R.E., J.T. Sherman, and J. Dufour. 2001. Profiling ALACEs and other advances in autonomous subsurface floats. *Journal of Atmospheric and Oceanic Technology* 18(6):982–993, https://doi.org/10.1175/1520-0426(2001)018<0982:PAAOAI>2.0.CO;2.

Hoskins, B.J., and F.P. Bretherton. 1972. Atmospheric frontogenesis models: Mathematical formulation and solution. *Journal of the Atmospheric Sciences* 29:11–37, https://doi.org/10.1175/1520-0469(1972)029<0011:AFMMFA>2.0.CO;2.

Hughes, K.G., J.N. Moum, and D.L. Rudnick. 2023. A turbulence data reduction scheme for autonomous and expendable profiling floats. *Ocean Science* 19(1), https://doi.org/10.5194/os-19-193-2023.

Johnston, T.M.S., D.L. Rudnick, N. Brizuela, and J.N. Moum. 2020. Advection by the North Equatorial Current of a cold wake due to multiple typhoons in the western Pacific: Measurements from a profiling float array. *Journal of Geophysical Research: Oceans* 125(4):e2019JC015534, https://doi.org/10.1029/2019JC015534.

Johnston, T.M.S., D.L. Rudnick, and E. Pallàs-Sanz. 2011. Elevated mixing at a front. *Journal of Geophysical Research: Oceans* 116(C11), https://doi.org/10.1029/2011JC007192.

Johnston, T.M.S., S. Wang, C.-Y. Lee, J.N. Moum, D.L. Rudnick, and A. Sobel. 2021. Near-inertial internal wave propagation in the wake of Super Typhoon Mangkhut: Measurements from a profiling float array. *Journal of Geophysical Research: Oceans* 126(2):e2020JC016749, https://doi.org/10.1029/2020JC016749.

Moum, J.N., and R.G. Lueck. 1985. Causes and implications of noise in oceanic dissipation measurements. *Deep Sea Research Part A* 32:379–390, https://doi.org/10.1016/0198-0149(85)90086-X.

Moum, J.N., A. Perlin, J.D. Nash, and M.J. McPhaden. 2013. Seasonal sea surface cooling in the equatorial Pacific cold tongue controlled by ocean mixing. *Nature* 500:64–67, https://doi.org/10.1038/nature12363.

Moum, J.N., D.L. Rudnick, and E.L. Shroyer, K.G. Hughes, B.D. Reineman, K. Grindley, J.T. Sherman, P. Vutukur, C. Van Appledorn, K. Latham, and others. 2022. Flippin' χSOLO, an upper ocean autonomous turbulence-profiling float. *Journal of Atmospheric and Oceanic Technology* 40(5):629–644, https://doi.org/10.1175/JTECH-D-22-0067.1.

Rudnick, D.L. 2001. On the horizontal variability of the upper ocean. Pp. 87–93 in *Proceedings of the 12th 'Aha Huliko'a Hawaiian Winter Workshop*, P. Müller and D. Henderson, eds.

Sanabia, E.R., and S.R. Jayne. 2020. Ocean observations under two major hurricanes: Evolution of the response across the storm wakes. *AGU Advances* 1(3):e2019AV000161, https://doi.org/10.1029/2019AV000161.

Warner, S.J., and J.N. Moum. 2019. Feedback of mixing to ENSO phase change. *Geophysical Research Letters* 46(23):13,920–13,927, https://doi.org/10.1029/2019GL085415.

AUTHORS

T.M. Shaun Johnston (shaunj@ucsd.edu), **Daniel L. Rudnick**, **Benjamin D. Reineman**, **Kyle Grindley**, **Michael McClune**, and **Jeffrey Sherman**, all at Scripps Institution of Oceanography, University of California San Diego, La Jolla, CA, USA. **James N. Moum**, **Emily L. Shroyer**, **Kenneth G. Hughes**, **Pavan Vutukur**, **Craig Van Appledorn**, **Kerry Latham**, **and Aurélie J. Moulin**, all at College of Earth, Ocean, and Atmospheric Sciences, Oregon State University, Corvallis, OR, USA.

The Epsilometer on Argo Floats

Arnaud Le Boyer, C. Andrew Parlier, Matthew H. Alford, Nicole Couto, Mike Goldin, Sean Lastuka, Sara Goheen, Mai Bui, San Nguyen, and Charlotte Bellerjeau

Our group has integrated the epsilometer, a microstructure sensor, onto an APEX Argo float as a part of Argo-mix, a new branch of the Argo mission. Argo floats are designed to be deployed for years, so integrated sensors must adapt to the life expectancy and mission of the floats. The microstructure-equipped float can measure turbulent dissipation rate (ε) and temperature gradient dissipation rate (χ) above 10^{-10} W kg^{-1} and K^2 s^{-1}, respectively. We are currently testing onboard processing and communication protocols on the float.

INTRODUCTION

The Argo community has identified ocean mixing measurements as an achievable scientific goal of the Argo mission (Roemmich et al., 2019). This new branch, named Argo-mix, would provide the scientific community repeated microstructure measurements at a global scale. These measurements would offer insights into the impact of ocean mixing on water mass transformations, air-sea interactions, and a plethora of other processes (Garabato and Meredith, 2022). New sensors should be low power and resilient so their integration does not modify the life expectancy or the core mission of a float. New sensors should also represent a manageable fraction of a float's price in order to achieve global-scale measurements. Microstructure sensor integration with an Argo float raises a number of challenges that our group is trying to overcome using our custom microstructure sensor: the epsilometer.

The epsilometer ("epsi"; Figure 1a) measures χ and ε, the thermal and kinetic energy dissipation rates from temperature gradient spectra for vertical shear spectra, respectively (Le Boyer et al., 2021). The shear probes, the FP07 temperature sensors, and the electronics are fabricated in house following techniques historically developed by Michael Gregg (Applied Physics Laboratory/University of Washington). For the Argo float integration, epsi samples three channels (one shear, one temperature, one axis of acceleration) at 24-bit

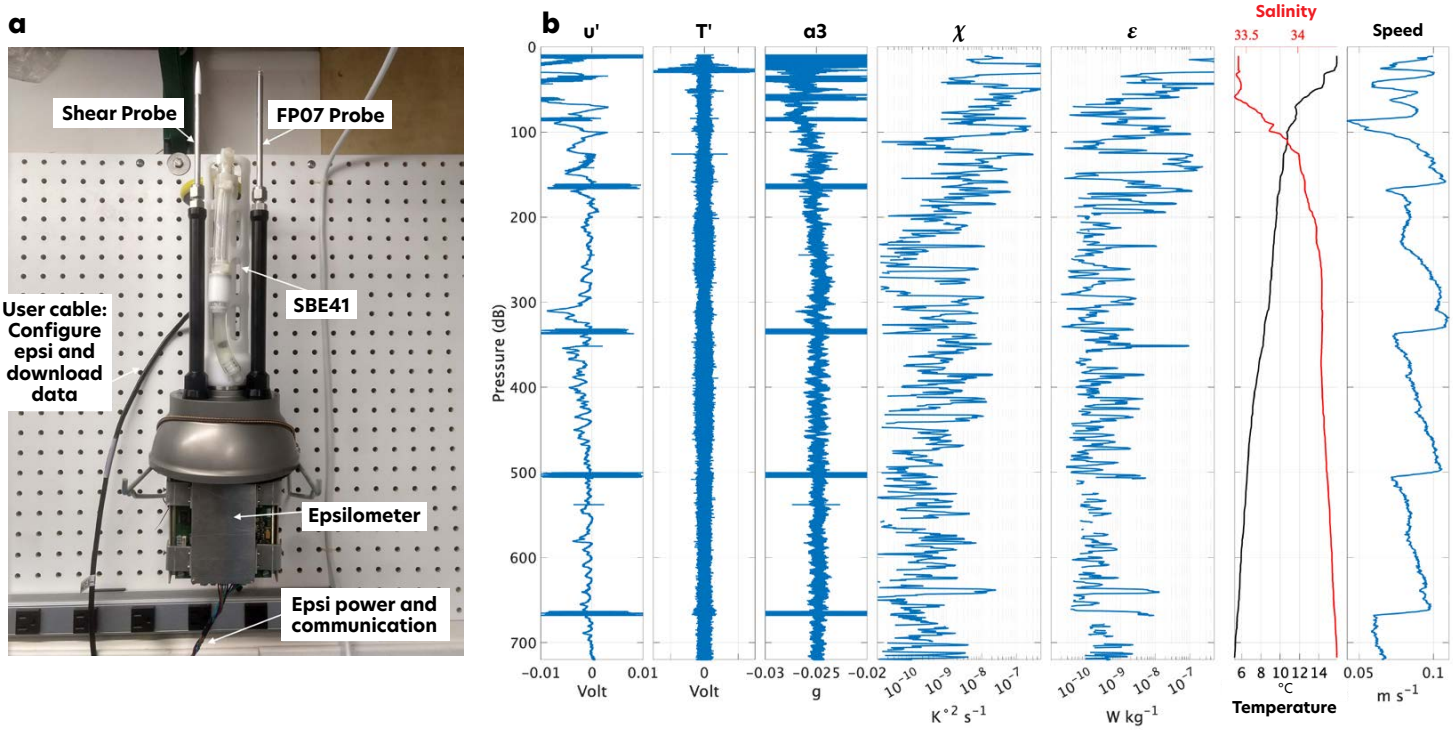

FIGURE 1. (a) The epsilometer inside its case mounted on the chassis of the APEX CTD (SBE 41). On the end cap, the shear probe and the FP07 thermistor stand above the CTD intake. (b) Raw data profiles from the shear probe (u'), the FP07 (T'), the accelerometer (a3). Profiles of χ and ε and T-S and speed profiles from the CTD.

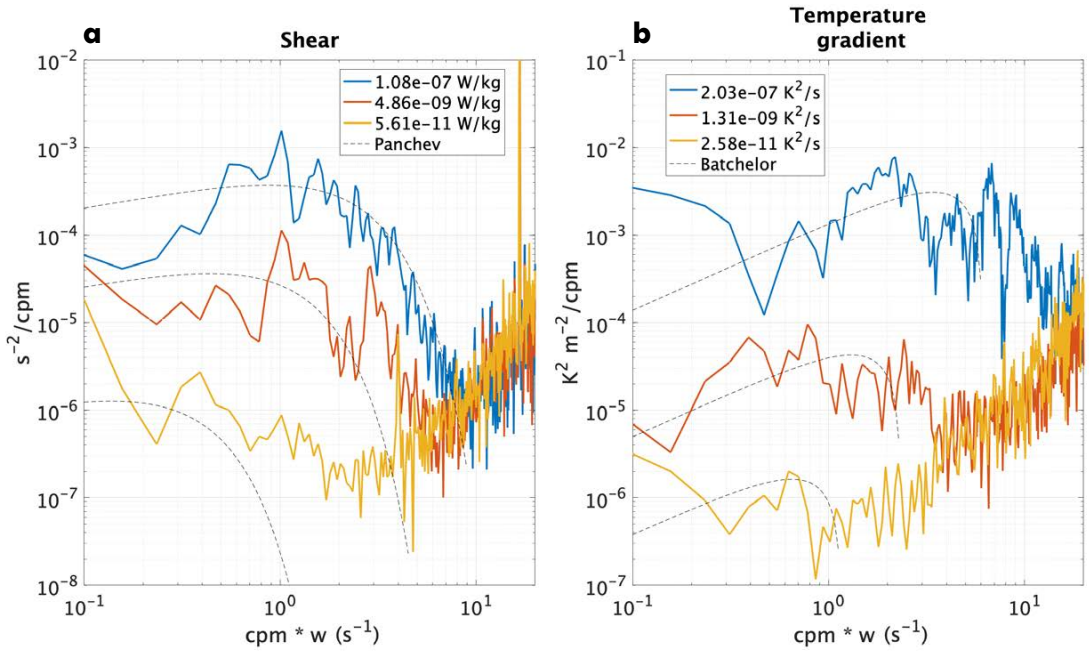

FIGURE 2. (a) Vertical shear spectra from the shear probe for increasing values of ε. (b) Temperature gradient spectra from the FP07 thermistor for increasing values of χ. Note the x-axis is a frequency axis so the spectra are aligned.

precision and a 160 Hz sampling frequency. The raw data are then recorded to a microSD card and processed onboard into ε and χ values. These data are stored in 25 kB packages for Iridium satellite telemetry.

APEX floats are autonomous, neutrally buoyant drifters used in support of the international Argo program (Sanford et al., 2005). They use a variable buoyancy engine to surface on a programmed schedule, returning temperature (T) and salinity (S) profiles via satellite. The floats and the communication protocol between epsi and the APEX controller (APF11) are provided by Dana Swift and Steve Riser (University of Washington).

In a standard Argo mode, the float descends to a depth target (usually 1,000 m), remains at depth for few days, and descends to 2,000 m before ascending to the surface while collecting T and S data, which are sent via Iridium satellite. While ascending, the buoyancy pump controls the vertical speed with 30 s buoyancy nudges, creating a sawtooth pattern in the vertical speed profile (Figure 1b). During the buoyancy nudges, float vibrations pollute microstructure shear measurements (Figure 1b). Epsi can sample during the ascent phase between the buoyancy nudges and produce ε and χ profiles (Figure 1b).

Our electronic boards are clamped on the chassis of the CTD frame (Figure 1a), and stand-offs position the probes a few inches above the CTD. Epsi collects the CTD data at the same time as the APF11. Epsi communicates with APF11 through a low-energy communication port. Epsi consumes 45 mW in sleep mode and approximately 250 mW when sampling. This is about 1.3 kJ for a 3 h cycle when profiling above 1,000 m, which represents about 10% of the 15 kJ the APEX float requires for one cycle.

SENSITIVITY RANGE

In February 2022, we deployed a stand-alone version of the APEX-epsi. The goal of this test is to assess the feasibility of microstructure measurements when profiling "à la Argo." The epsi was powered by the float's battery. It did not communicate with the APF11 and did not process the data onboard during this deployment.

The float profiled to approximately 800 m depth during this test (Figure 1b). At depths of 680 m, 500 m, 320 m, and 180 m, the buoyancy pump increased the vertical speed of the float to 10 cm s^{-1} and dominated the shear and acceleration signals (u' and a3, Figure 1b). While the float ascent rate was slow (5–10 cm s^{-1}, Figure 1b) compared to speeds of profiling platforms often used to carry microstructure sensors (50 cm s^{-1}, Le Boyer et al. 2021), the microstructure channels (shear and temperature gradient) show a sensitive range for $\varepsilon > 10 \times 10^{-10}$ W kg^{-1} and $\chi > 10 \times 10^{-10}$ K^2 s^{-1} (Figure 2).

DISCUSSION

The sensitive range presented in Figure 2 confirms the feasibility of measuring turbulence on a core Argo float. The onboard processing and communication with the APF11 are being tested. Once the onboard processing is fully tested, three APEX-epsi floats will be used in a pilot experiment that will provide insight into shear probe endurance. These probes are still fragile, and our group is investigating the use of a plastic material with piezoelectric properties (polyvinylidene fluoride) in order to increase the resilience of these probes.

The ongoing APEX-epsi integration is paving the way for other autonomous platforms such as the recent DeepSOLO float, also part of the Argo fleet. These floats are able to

dive to 6,000 m and could sample the enhanced mixing above rough topographies (Garabato and Meredith, 2022). The onboard processing and communication protocol achieved with APEX-epsi simplifies this future integration because the main challenges will be related to the mechanical design of a buoyantly neutral epsilometer that could support abyssal pressures.

REFERENCES

Garabato, A.N., and M. Meredith. 2022. Ocean mixing: Oceanography at a watershed. Pp. 1–4 in *Ocean Mixing: Drivers, Mechanisms, and Impacts*, M. Meredith and A. Naveira Garabato, eds, Elsevier, https://doi.org/10.1016/B978-0-12-821512-8.00008-6.

Le Boyer, A., M.H. Alford, N. Couto, M. Goldin, S. Lastuka, S. Goheen, S. Nguyen, A.J. Lucas, and T.D. Hennon. 2021. Modular, flexible, low-cost microstructure measurements: The epsilometer. *Journal of Atmospheric and Oceanic Technology* 38(3):657–668, https://doi.org/10.1175/JTECH-D-20-0116.1.

Roemmich, D., M.H. Alford, H. Claustre, K. Johnson, B. King, J. Moum, P. Oke, W.B. Owens, S. Pouliquen, S. Purkey, and others. 2019. On the future of Argo: A global, full-depth, multi-disciplinary array. *Frontiers in Marine Science* 6:439, https://doi.org/10.3389/fmars.2019.00439.

Sanford, T.B., J.H. Dunlap, J.A. Carlson, D.C. Webb, and J.B. Girton. 2005. Autonomous velocity and density profiler: EM-APEX. Pp. 152–156 in *Proceedings of the IEEE/OES Eighth Working Conference on Current Measurement Technology, 2005*, June 28–29, 2005, Southampton, UI, IEEE, https://doi.org/10.1109/CCM.2005.1506361.

AUTHORS

Arnaud Le Boyer (aleboyer@ucsd.edu), **C. Andrew Parlier**, **Matthew H. Alford**, **Nicole Couto**, **Mike Goldin**, **Sean Lastuka**, **Sara Goheen**, **Mai Bui**, **San Nguyen**, and **Charlotte Bellerjeau**, all at Scripps Institution of Oceanography, University of California San Diego, La Jolla, CA, USA.

Two Quality-Control Metrics for Dissipation Estimates

Rolf G. Lueck

The very large volume of turbulence shear data that will be collected with autonomous vehicles will require robust and autonomous data processing. In particular, the quality of a measurement must be quantified, so that poor measurements can be rejected. Such quality control requires an estimate of the statistical uncertainty of a turbulence shear measurement, both with respect to its variance and its spectral shape. The statistical uncertainty of a dissipation estimate depends on the length of data used for an estimate and the uncertainty of a spectrum of shear depends on the number of FFT segments used to form the spectrum. It has recently been shown that both of these uncertainties have a log-normal probability density function (Lueck, 2022a,b). This article presents some examples of how the statistical nature of a measurement can be used to quantify its quality.

BACKGROUND

Turbulence shear is a statistical process. Measuring turbulence shear with a shear probe is a sampling of this statistical process. The quantities that are derived from a measurement, such as its variance and its spectrum, are unbiased if the probe is calibrated, but the sample variance (or spectrum) will differ from the population (or true) variance or spectrum because of the limited amount of data in a sample. In isotropic turbulence (Taylor, 1935; Pope, 2009), the rate of dissipation is related to the variance of shear by

$$\epsilon = \frac{15}{2}\nu\overline{\left(\frac{\partial w}{\partial x}\right)^2} = \frac{15}{2}\nu\int_0^\infty \Psi(k)\,\mathrm{d}k \approx \frac{15}{2}\nu\int_0^{k_u} \Psi(k)\,\mathrm{d}k \qquad (1)$$

where ν is the kinematic viscosity, w is any velocity component orthogonal to the direction of profiling, x is any direction of profiling, $\Psi(k)$ is the spectrum of shear, k is the wavenumber in the x-direction, and $k_u < \infty$ is an upper wavenumber imposed by practical considerations, such as the avoidance of noise and vibrational contamination in a shear-probe signal.

A comparison of the logarithm of ε, derived from four co-located shear probes in a tidal boundary layer, shows that the differences between the probes are normally distributed. The variance of the differences decreases with increasing averaging length according to

$$\sigma^2_{\ln\epsilon} = \frac{5.5}{1+\left(\hat{L}_f/4\right)^{7/9}}\ ,\quad \hat{L}_f \equiv \hat{L}\,V_f^{3/4} = \frac{L}{L_K}V_f^{3/4} \qquad (2)$$

where L is the dimensional length of an ε estimate, $L_K = (\nu^3/\varepsilon)^{1/4}$ is the Kolomogorov length, and V_f is the fraction of the variance resolved by truncating the spectrum at an upper wavenumber of k_u (1). $\sigma_{\ln\,\varepsilon}$ can then be used to derive a confidence interval of a dissipation estimate. For example, the 95% confidence interval is ε exp (±1.96 $\sigma_{\ln\,\varepsilon}$).

A comparison of the logarithm of the spectra of shear from the four co-located probes shows that the differences are also normally distributed. The variance of the spectral differences decreases with increasing number of FFT-segments, N_f, that are used to estimate the spectrum according to

$$\sigma^2_{\ln\Psi} = \frac{5}{4}\left(N_f - N_V\right)^{-7/9} + 0.015 \approx \frac{5}{4}\left(N_f - N_V\right)^{-7/9} \qquad (3)$$

where N_V is the number of vibration or other signals that were used to clean the shear spectrum. $\sigma_{\ln\Psi}$ can then be used to derive a confidence interval of a spectrum of shear.

DISSIPATION RATIOS

It is now possible to compare two simultaneous dissipation estimates to decide if their ratio is within the bounds of the statistical uncertainty of an estimate, or if one is too large because of some sort of signal contamination (which adds variance to the shear). That is, (2) can be used for outlier detection. The 95% confidence interval for the geometric mean of a pair of dissipation estimates is

$$\sqrt{\epsilon_1\epsilon_2}\,\exp\left(\pm 1.96\,\sigma_{\ln\epsilon}\sqrt{1/2}\right) \qquad (4)$$

where the factor of $\sqrt{1/2}$ accounts for the one degree of freedom that is consumed by estimating the mean. Thus, there is only a 5% probability that the ratio of a pair of estimates exceeds

$$\exp\left(\pm 1.96\,\sigma_{\ln\epsilon}\sqrt{2}\right) \qquad (5)$$

It is likely that the larger of the two is erroneous because signal contamination (from vibrations or collisions with plankton) serves to increase the variance of shear. If there

are more than two shear-probe signals, then the estimates should be sorted in ascending order. The ratio of the largest to the smallest should be tested first. If this ratio is less than (5), then all other pairs will also pass this test. If not, the second largest and the smallest should be tested next, until a pair passes the test or until all pairs have been tested. The larger of a pair that fails this test should be flagged for rejection.

SPECTRAL QUALITY

The rate of dissipation is usually estimated using the approximation (the rightmost part) of (1). The logarithm of each spectral value has a standard deviation given by the square root of (3) and this can be used to set a limit on the departure of a measured spectrum from a reference spectrum. Let the number of spectral values that are used in an estimate of the shear variance be N_s. The mean absolute deviation ($\mathrm{MAD}_{\ln\Psi}$) of the logarithm of the spectral values, used in a dissipation estimate, from the logarithm of a reference spectrum, such as the Nasmyth spectrum (Lueck, 2022b), should not exceed

$$\sigma_{\ln\Psi}\, T_M = \sigma_{\ln\Psi}\left(0.8 + \sqrt{\frac{1.56}{N_s}}\right) \tag{6}$$

for 97.5% of the estimates that are based on N_s spectral values. The factor T_M is determined from a sampling of a normal process with a standard deviation of 1 (Figure 1). Therefore, a measure of the quality of a spectrum, over the wavenumber range used to make an e estimate, is

$$Q_M = \frac{\mathrm{MAD}_{\ln\Psi}}{\sigma_{\ln\Psi}}\,\frac{1}{T_M} \tag{7}$$

and Q_M should be smaller than 1 for 97.5% of the spectra. Dissipation estimates made from spectra with $Q_M > 1$ should be rejected.

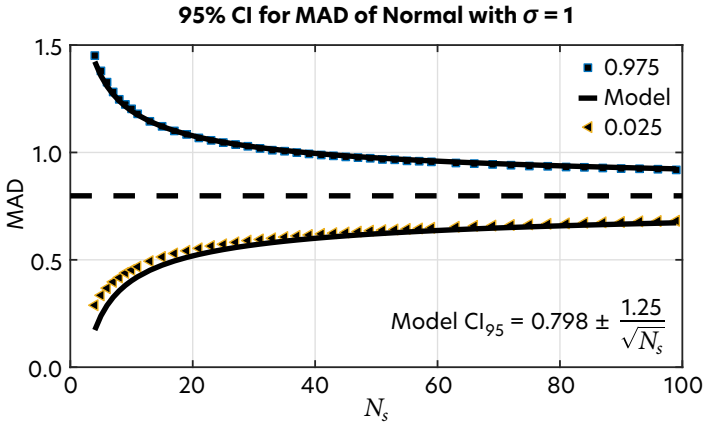

FIGURE 1. The 95% confidence interval of the mean absolute deviation (MAD) of N_s samples drawn from a normal population with a standard deviation of 1.

REFERENCES

Lueck, R.G. 2022a. The statistics of turbulence measurements. Part 1: Shear variance and dissipation rates. *Journal of Atmospheric and Oceanic Technology* 39(9):1,259–1,271, https://doi.org/10.1175/JTECH-D-21-0051.1.

Lueck, R.G. 2022b. The statistics of turbulence measurements: Shear spectra and a new spectral model. *Journal of Atmospheric and Oceanic Technology* 39(9):1,273–1,282, https://doi.org/10.1175/JTECH-D-21-0050.1.

Pope, S.B. 2009. *Turbulent Flows*. Cambridge University Press, 802 pp., https://doi.org/10.1017/CBO9780511840531.

Taylor, G. 1935. Statistical theory of turbulence. *Proceedings of the Royal Society A* 151:421–444, https://doi.org/10.1098/rspa.1935.0158.

AUTHOR

Rolf G. Lueck (rolf@rocklandscientific.com), Rockland Scientific International, Inc.

Turbulence Measurements from a Medium-Diameter Autonomous Underwater Vehicle in an Island Wake

Sophia T. Merrifield, T.P. Welch, and Rolf Lueck

Measurements of turbulent dissipation and stratification were collected from a medium diameter autonomous underwater vehicle (AUV) sampling in the near-field oceanic wake of Rota, a small island in the Western Pacific. Ground truth measurements were collected from a vertical microstructure profiler (VMP) operated within 10 km of the AUV. Strong agreement is found between the platforms down to 10^{-9} W kg^{-1}, which is considered the noise floor of the AUV due to vehicular vibrations. The speed, persistence, and depth-variable capabilities of the AUV provide important measurements of horizontal structures that cannot be resolved from vertical profilers.

BACKGROUND

Microstructure measurements from AUVs began in the 1970s when scientists used metal-film temperature and velocity sensors on the Self-Propelled Underwater Research Vehicle (SPURV) operated by the University of Washington Applied Physics Laboratory (Irish and Nodland, 1978). Advances in processing techniques led to the reduction of host vehicle contamination using coherent subtraction methods (Levine and Lueck, 1999; Goodman et al., 2006). Compared to AUVs, buoyancy-driven gliders have lower noise floors, $O(10^{-11}$ W kg$^{-1})$ (Wolk et al., 2009) and can operate longer (Rainville et al., 2017). Scientific applications include sampling overflows (Fer et al., 2014) and near-surface dynamics (St. Laurent and Merrifield, 2017).

Propeller-driven vehicles provide faster survey capabilities but have much higher vibrational noise than buoyancy driven systems, mainly due to their propulsion system. Turbulence measurements have been collected from several different propeller-driven AUVs, including: the US Navy's Large Diameter Unmanned Underwater Vehicle with a length of 7.6 m (Levine and Lueck, 1999); Florida Atlantic University's AUV with a length of 2.4 m (Dhanak and Holappa, 1999); a small-diameter Remote Environmental Measuring Unit (REMUS) with a length of 2 m (Goodman and Wang, 2009); a medium-diameter REMUS with a length of 4 m (Fisher et al., 2018); and an OceanScan Marine Systems and Technology AUV with a length of 2.6 m (Kolås et al., 2022).

Here we document the sensor integration and field operation of a REMUS 600 that we used to sample the near-field wake of an island.

AUV INTEGRATION AND DATA PROCESSING

The REMUS 600 is a medium-diameter AUV that has a length of 4.3 m, a diameter of 0.7 m, and a weight of 530 lbs in air. An SBE49 FastCAT CTD (Sea-Bird Scientific, Bellevue, WA) and a MicroRider (MR) (Rockland Scientific, Victoria, BC) were integrated into the nose of the AUV to measure stratification and turbulent dissipation, respectively (Figure 1a). The SBE49 is controlled via a Robot Operating System (ROS) node running on the AUV's backseat computer (ADLE3800). The ROS node records SBE49 data at 9 Hz, in tandem with the vehicular state information from the front seat computer.

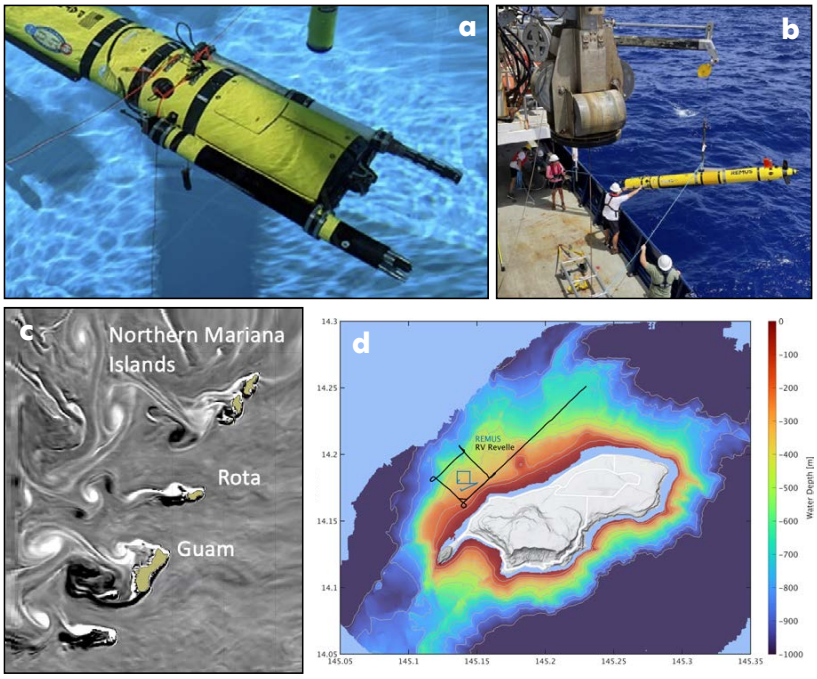

FIGURE 1. (a) The MicroRider and an SBE49 FastCAT CTD mounted on the autonomous underwater vehicle (AUV) REMUS 600. (b) A deployment of the REMUS 600. (c) Rota in the Western Pacific in a model field of relative vorticity (courtesy Harper Simmons, APL/UW) showing the wakes on the western side. (d) Bathymetry around Rota and the track of REMUS (blue) and R/V *Revelle* (black) during one AUV sortie.

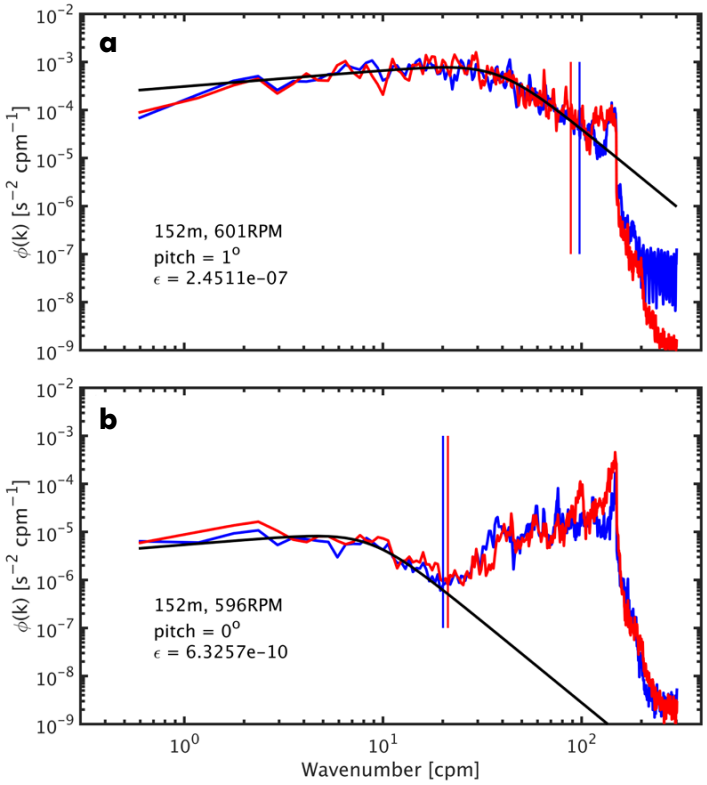

FIGURE 2. Example shear spectra from a region of high (a) and low (b) dissipation rates from probes 1 (red) and 2 (blue).

The MR sampled at 1,024 Hz, recorded its data internally, and was powered from the AUV +12 V guest port power supply. The ROS node synchronizes the MR and the ADLE3800 clocks prior to every logging session. The MR carries two orthogonally oriented airfoil shear probes, two FP07 thermistors, a pressure sensor, a roll and tilt sensor, an electromagnetic current (EM) meter, and two orthogonal vibration sensors.

Microstructure records are evaluated over 8-second intervals using a 1-second fast Fourier Transform length and a 50% overlap. One second corresponds to 1.7–2.2 m spatial intervals based on the AUV survey speed during level and inclined runs, respectively. Vehicle vibrations are removed using the coherent method of Goodman et al. (2006). Frequency spectra are converted to wavenumber spectra using the vehicle velocity measured by the EM sensor. The shear data are high-pass filtered with a cutoff of 0.4 Hz, and cleaned wavenumber spectra are integrated to 115 cpm or to the wavenumber minimum of a 3rd-order polynomial fit to the spectrum. Spectral quality is evaluated relative to the Nasmyth spectrum (Nasmyth, 1970; Oakey, 1982) and a noise floor of 10^{-9} W kg^{-1} is estimated empirically for the AUV-based measurements. Electrically and mechanically induced noise was investigated extensively. The propulsion is the main source of noise inducing a vibration at 40 Hz and many of its harmonics, while some noise was also induced by the SBE49 pump. After vibration-coherent contamination is removed from the shear-probe spectra, they agree well with the Nasmyth reference spectrum for rates ranging from ~10^{-9} to ~10^{-7} W kg^{-1} (Figure 2). Ascents and descents provided similar data quality.

RESULTS

An Office of Naval Research-sponsored Department Research Initiative, the Island Arc Turbulent Eddy Regional Exchange, focuses on submesoscale dynamics in the wake of islands in the Western Pacific (Figure 1c). R/V *Roger Revelle* was deployed in April–May 2022 to study the wake of Rota, an island of dimensions 20 km × 5 km that sits in the predominantly westward-flowing Northern Equatorial Current, using both the REMUS 600 and a conventional vertical microstructure profiler (VMP). To reduce the number of GPS surfacings for navigational fixes, the AUV operated in water that was sufficiently shallow for bottom tracking (<400 m). The AUV sampled the perimeter of a 1 km × 1 km square box conducting horizontal surveys at depths of 15, 50, 100, 150, and 200 m (Figures 1d and 3). Between each constant depth box, the AUV surfaced for a GPS fix.

The AUV measurements are validated by comparing them to simultaneous VMP profiles obtained by tow-yo'ing from the stern of R/V *Revelle* (Figure 1d, black dots). The VMP was equipped with a high-accuracy CT sensor to also provide salinity profiles. Temperature, salinity, and turbulent kinetic energy dissipation (ε) (Figure 3a–c) measurements as a function of depth show strong agreement between the two platforms, particularly when the AUV and the research vessel were within 5 km of each other (Figure 3d). Dissipation rate are enhanced ($\varepsilon > 10^{-8}$ W kg^{-1}) in the upper 50–75 m with a layer of lower dissipation ($\varepsilon \sim 10^{-10} - 10^{-9}$ W kg^{-1}) between 75 m and 125 m. At greater depths, dissipation rates grow due to a strong shear layers in the salinity maximum (not shown).

REFERENCES

Dhanak, M.R., and K. Holappa. 1999. An autonomous ocean turbulence measurement platform. *Journal of Atmospheric and Oceanic Technology*, 16(11):1,506–1,518, https://doi.org/10.1175/1520-0426(1999)016<1506:AAOTMP>2.0.CO;2.

Fer, I., A.K. Peterson, and J.E. Ullgren. 2014. Microstructure measurements from an underwater glider in the turbulent Faroe Bank Channel overflow. *Journal of Atmospheric and Oceanic Technology* 31(5):1,128–1,150, https://doi.org/10.1175/JTECH-D-13-00221.1.

Fisher, A.W., N.J. Nidzieko, M.E. Scully, R.J. Chant, E.J. Hunter and P.L. Mazzini. 2018. Turbulent mixing in a far-field plume during the transition to upwelling conditions: Microstructure observations from an AUV. *Geophysical Research Letters* 45(18):9,765–9,773, https://doi.org/10.1029/2018GL078543.

Goodman, L., E.R. Levine, and R.G. Lueck. 2006. On measuring the terms of the turbulent kinetic energy budget from an AUV. *Journal of Atmospheric and Oceanic Technology* 23(7):977–990, https://doi.org/10.1175/JTECH1889.1.

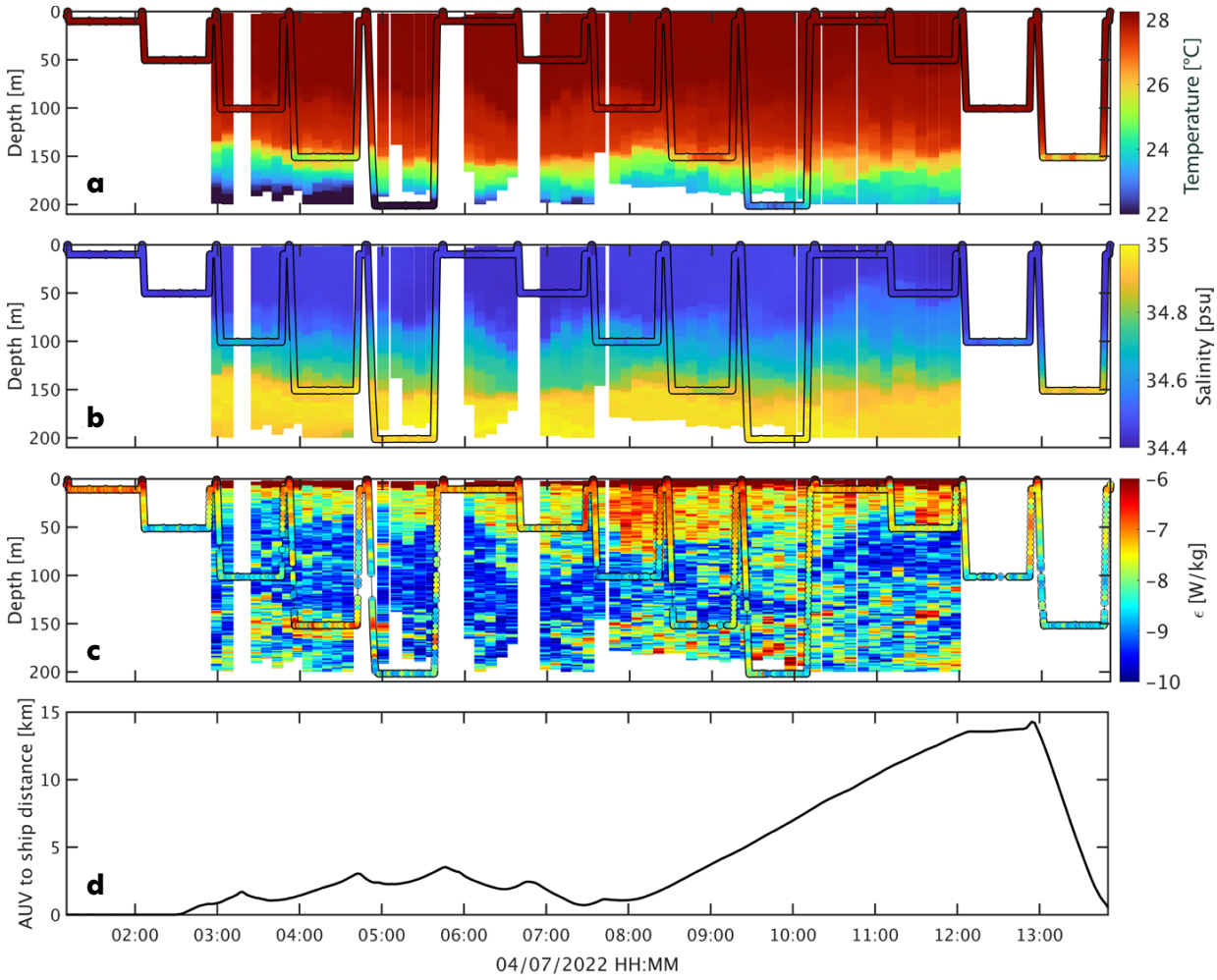

FIGURE 3. (a) Temperature, (b) salinity, and (c) dissipation rates measured with the vertical microstructure profiler (background) and the MicroRider (black frame) integrated into the AUV. (d) The distance between the AUV and the surface ship.

Goodman, L., and Z. Wang. 2009. Turbulence observations in the northern bight of Monterey Bay from a small AUV. *Journal of Marine Systems* 77(4):441–458, https://doi.org/10.1016/j.jmarsys.2008.11.004.

Irish, J., and W. Nodland. 1978. Evaluation of metal-film temperature and velocity sensors and the stability of a self-propelled research vehicle for making measurements of ocean turbulence. In OCEANS'78, September 6–8, 1978, Washington, DC, IEEE, https://doi.org/10.1109/OCEANS.1978.1151113.

Kolås, E.H., T. Mo-Bjørkelund, and I. Fer. 2022. Turbulence measurements from a light autonomous underwater vehicle. *Ocean Science* 18(2):389–400, https://doi.org/10.5194/os-18-389-2022.

Levine, E.R., and R.G. Lueck. 1999. Turbulence measurement from an autonomous underwater vehicle. *Journal of Atmospheric and Oceanic Technology* 16(11):1,533–1,544, https://doi.org/10.1175/1520-0426(1999)016<1533:TMFAAU>2.0.CO;2.

Nasmyth, P.W. 1970. *Oceanic Turbulence*. PhD Thesis, University of British Columbia.

Oakey, N. 1982. Determination of the rate of dissipation of turbulent energy from simultaneous temperature and velocity shear microstructure measurements. *Journal of Physical Oceanography* 12(3):256–271, https://doi.org/10.1175/1520-0485(1982)012<0256:DOTROD>2.0.CO;2.

Rainville, L., J.I. Gobat, C.M. Lee, and G.B. Shilling. 2017. Multi-month dissipation estimates using microstructure from autonomous underwater gliders, *Oceanography* 30(2):49–50, https://doi.org/10.5670/oceanog.2017.219.

St. Laurent, L., and S. Merrifield. 2017. Measurements of near-surface turbulence and mixing from autonomous ocean gliders. *Oceanography* 30(2):116–125, https://doi.org/10.5670/oceanog.2017.231.

Wolk, F., R. Lueck, and L.S. Laurent. 2009. Turbulence measurements from a glider. In *OCEANS 2009*, October 26–29, 2009, Biloxi, MS, IEEE, https://doi.org/10.23919/OCEANS.2009.5422413.

ACKNOWLEDGMENTS

We thank the Office of Naval Research program managers Scott Harper, Emily Shroyer, and Louis St. Laurent. The crew of the R/V *Roger Revelle* was instrumental in deployment and recovery of the AUV. This work would not be possible without the efforts of Scripps Institution of Oceanography engineers Sean McPeak, Bob Hess, Nixon Carruthers, and Jacob Springman.

AUTHORS

Sophia T. Merrifield (smerrifield@ucsd.edu), Marine Physical Laboratory, Scripps Institution of Oceanography, University of California San Diego, La Jolla, CA, USA. **T.P. Welch**, College of Earth, Ocean, and Atmospheric Sciences, Oregon State University, Corvallis, OR, USA. **Rolf Lueck**, Rockland Scientific, Victoria, BC, Canada.

Measurements of ε Featuring Flippin' χSOLO

James N. Moum, Kenneth G. Hughes, Daniel L. Rudnick, and Emily L. Shroyer

Field trials of a newly developed upper ocean autonomous turbulence profiler, Flippin' χSOLO (FχS) included 3.5 days of turbulence profiling using two FχS units plus the Chameleon profiler deployed from a ship. Histograms of turbulence kinetic energy dissipation rate (ε) from below the mixed layer differ due to particular profiler characteristics. Mean values agree within a factor of 2.

FLIPPIN' χSOLO

Flippin' χSOLO (FχS) is a modified SOLO-II float with an SBE Glider Payload CTD (GPCTD) and a fully integrated turbulence package that includes two airfoil probes (Osborn, 1974), two fast thermistors, and a pitot tube (Figure 1). The descriptor Flippin' refers to the engineering solution to the requirement of providing the turbulence sensors access to fluid undisturbed by the presence of communication antennae while profiling upward through the sea surface. Turbulence sensors and antennae must both be exposed at the sea surface, and they must not interact. Our solution was to house turbulence sensors at one end and antennae at the other. FχS flips at the sea surface following the upward profile to expose antennae for communications. It then flips at the bottom of each profile so that turbulence sensors lead on both ascending and descending profiles. The flip is achieved by shifting ballast (Johnston et al., 2023).

Field tests of FχS were conducted off the Oregon coast in May 2019 from R/V *Oceanus*. Two FχS units were deployed nearby each other while the ship stayed within 5 km of the units. Our turbulence profiler, Chameleon, was deployed from ship at the rate of ~7 profiles per hour to 200 m depth. The FχS units profiled at ~3 profiles per hour (ascents and descents) to nominally 100 m depth.

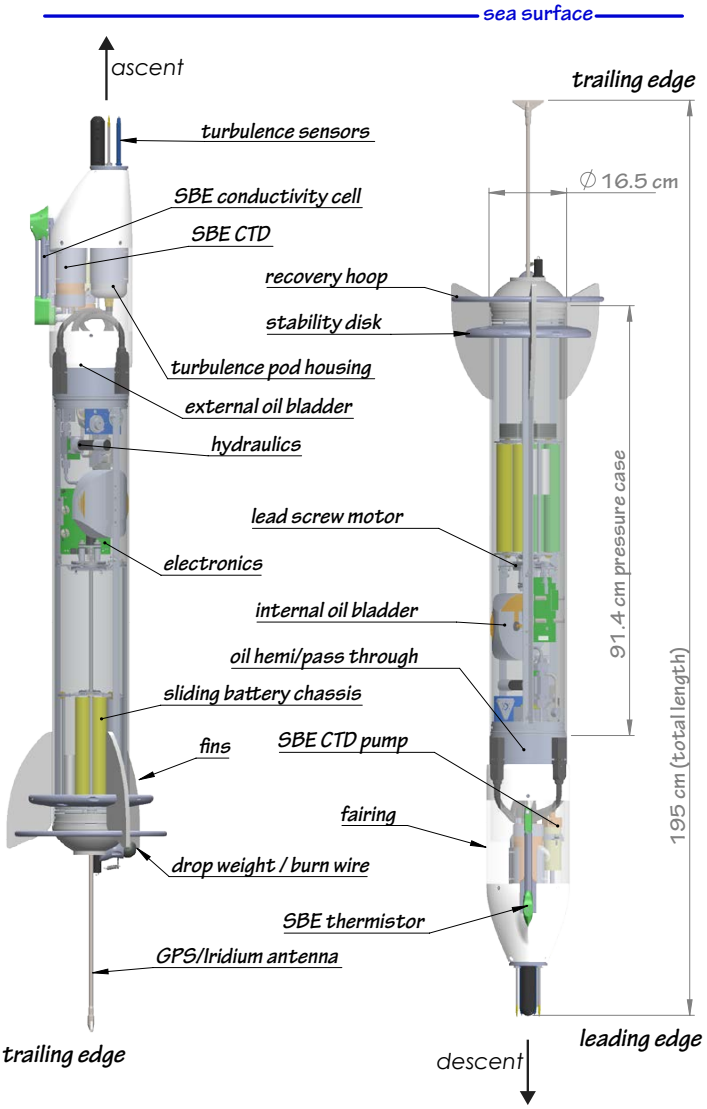

FIGURE 1. Schematic of Flippin' χSOLO.

COMPARATIVE HISTOGRAMS OF ε

Here we consider turbulence beneath the mixed layer and proceed with the assumption that the scale of atmospheric forcing is large relative to the spacings of the three turbulence profilers so that, in a statistical sense, they sample the same turbulence similarly forced. Image plots of ε show differences in part because of different profiling rates (Figure 2a,b vs. 2c) and in part due to different noise characteristics (Figure 2a vs. 2b).

Considerable variability appears in the shapes of the histograms (Figure 3) of ε from the three profilers over the depth range shown in Figure 2. This is principally because noise characteristics differ between profilers for a number of reasons. The data ranges and medians reflect these differences. However, mean values agree with 95% confidence. This suggests that the turbulence that matters, the most intense turbulence in these high kurtosis distributions, has been adequately sampled. The agreement is not perfect but within a factor of 2.

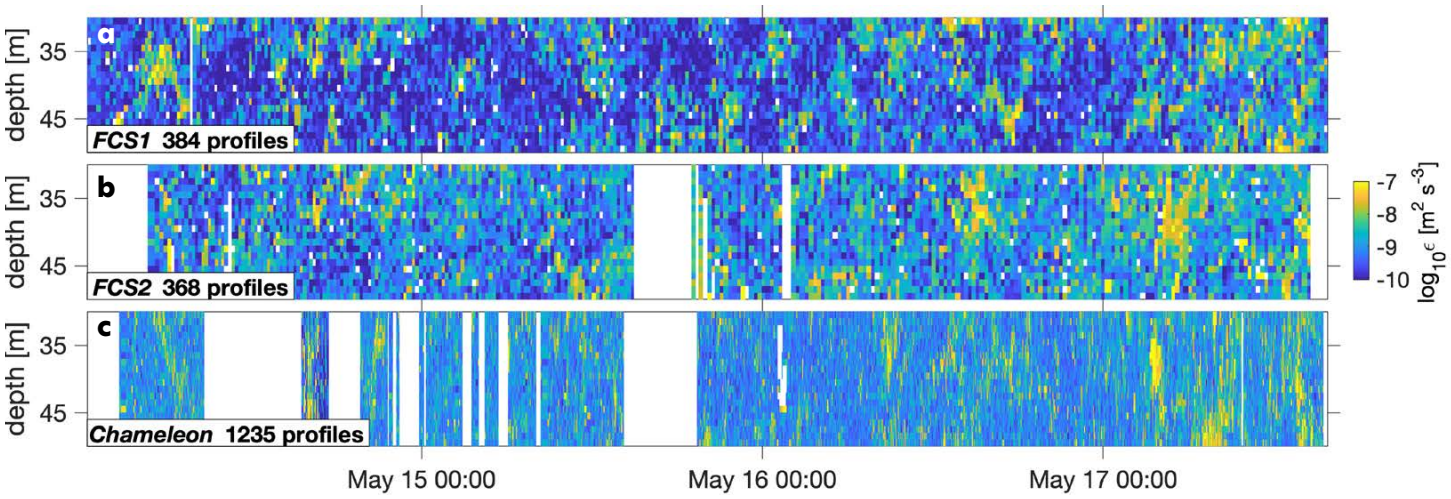

FIGURE 2. Image plots of ε over 20–60 m and 3.5 days from two FχS units and Chameleon while the ship remained within <5 km of the units.

Three independent findings indicate that coincident or near-coincident point measurements of geophysical turbulence cannot be expected to agree to better than a factor of 2. (1) Lueck (2023) demonstrates that nearly co-located airfoil probes in a high Re, likely stationary and homogeneous, turbulence yield estimates of ε that agree only to within a factor of 2. (2) Hughes and Moum (2023) show that only 71% of 77,000 independent estimates of ε from two co-located airfoil probes on FχS agree to within a factor of 2. (3) Inter-platform sampling of statistically similar geophysical turbulence indicates that considerable averaging (days) is required to reduce differences in mean values of ε to within a factor of 2 (Moum et al., 1995; Perlin and Moum, 2012).

As we proceed toward autonomous sampling of geophysical turbulence with limited resources and long intervals between profiles in a vast ocean, we need to consider sampling uncertainties. Platforms such as FχS offer ways to both sparsely sample the larger ocean and to densely sample subdomains of the ocean with the objective of defining sparse-sampling uncertainties.

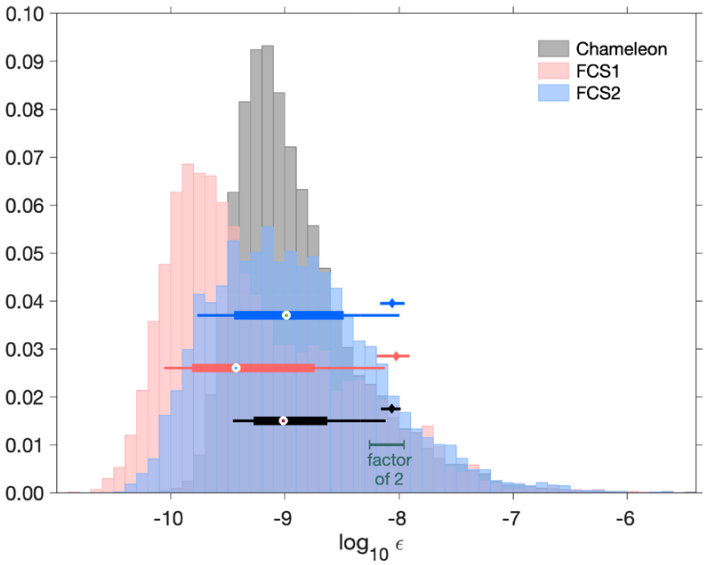

FIGURE 3. Histograms (normalized such that the sum of the bar heights = 1) of ε from the data in Figure 2. Thick bars denote 75% data range and thin bars 90% data range. Circles indicate medians. Diamonds are means of each distribution with bootstrapped 95% confidence intervals shown by the horizontal bars.

REFERENCES

Hughes, K.G., and J.N. Moum. 2023. Different approaches to onboard reduction of turbulence data: Pros and cons. Pp. 8–9 in *Microstructure Sensing from Autonomous Platforms*. Report of the Office of Naval Research Sponsored Workshop, E. Shroyer and L. St. Laurent, eds., May 2022, Lake Arrowhead, California.

Johnston, T.M.S., D.L. Rudnick, B.D. Reineman, K. Grindley, M. McClune, J. Sherman, J.N. Moum, E.L. Shroyer, K.G. Hughes, P. Vutukur, and others. 2023. Attitude of the Flippin' χSOLO. Pp. 10–13 in *Microstructure Sensing from Autonomous Platforms*. Report of the Office of Naval Research Sponsored Workshop, E. Shroyer and L. St. Laurent, eds., May 2022, Lake Arrowhead, California.

Lueck, R.G. 2023. Two quality-control metrics for dissipation estimates. Pp. 17–18 in *Microstructure Sensing from Autonomous Platforms*. Report of the Office of Naval Research Sponsored Workshop, E. Shroyer and L. St. Laurent, eds., May 2022, Lake Arrowhead, California.

Moum, J.N., M.C. Gregg, R.C. Lien, and M. Carr. 1995. Comparison of turbulence kinetic energy dissipation rate estimates from two ocean microstructure profilers. *Journal of Atmospheric and Oceanic Technology* 12(2):346–366, https://doi.org/10.1175/1520-0426(1995)012<0346:COTKED>2.0.CO;2.

Osborn, T.R. 1974. Vertical profiling of velocity microstructure. *Journal of Physical Oceanography* 4(1):109–115, https://doi.org/10.1175/1520-0485(1974)004<0109:VPOVM>2.0.CO;2.

Perlin, A., and J.N. Moum. 2012. Comparison of thermal variance dissipation rates from moored and profiling instruments at the equator. *Journal of Atmospheric and Oceanic Technology* 29:1,347–1,362, https://doi.org/10.1175/JTECH-D-12-00019.1.

AUTHORS

James N. Moum (jim.moum@oregonstate.edu) and **Kenneth G. Hughes**, both at College of Earth, Ocean, and Atmospheric Sciences, Oregon State University, Corvallis, OR, USA. **Daniel L. Rudnick**, Scripps Institution of Oceanography, University of California San Diego, La Jolla, CA, USA. **Emily L. Shroyer**, Oregon State University, Corvallis, OR, USA.

Dissipation, Diffusion, and Fine Structure

Thomas Osborn

OSBORN-COX

It probably goes back to Bob Stewart telling Walter Munk, who told Chip Cox about the turbulence measurements being carried out in Victoria, BC, Canada. Chip started doing some simple temperature profiling while planning a more sophisticated instrument. When shopping for a PhD project, I talked to Chip, and he showed me an intriguing idea for calculating the vertical diffusion coefficient for heat from detailed measurements of the temperature gradient.

The Osborn-Cox model for estimating the vertical diffusivity, suffers from at least two problems: (1) the lateral advection and diffusion of temperature fluctuations can be considerable, leading to a possible overestimate of the vertical diffusivity, and (2) it is very difficult to fully resolve the temperature gradient, leading to an underestimate.

At the time (1960s), conventional wisdom expected the diffusivity to be on the order of 1 in cgs units. My experience with the thesis data collected in the San Diego Trough, which was held to be a region of strong internal wave activity, suggested it would be difficult to get a number that large. It was also clear that thermistor response was a problem and that a substantial fraction of the variance in the gradient was attenuated by the boundary layer and thermal mass of the thermistor.

Upon graduation, we went to the University of British Columbia (UBC). The Institute of Oceanography at UBC was a wonderful place. There were excellent students, an active air-sea interactions program and easy access to ship time. In addition, everyone had an appointment in a university department. Physical oceanographers were in the physics department. Thus, I got to lecture a first-year course in mechanics for engineers. There's nothing like lecturing to teach oneself the subject.

AIRFOIL PROBES

Pat Nasmyth told me about the Ribner and Siddon development of the airfoil probe. Fortunately, Tom Siddon was in the mechanical engineering department at UBC and only two blocks away. He showed us how they made the probes that were used in air. Developing a probe that was sufficiently sensitive and yet waterproof took a while. Calibration, thermal sensitivity, spatial response, electronics, and free-fall vehicles were dealt with to some degree or another (later and much better by others). This measurement system now enables the global mapping of dissipation that Bob Stewart called for at the 1968 Turbulence Symposium at UBC.

The dissipation measurements led to a nice series of experiments. Bill Crawford's thesis on the Atlantic Equatorial Undercurrent was a major effort with exceptional results. The turbulence was clearly associated with the strong shear layers above and below the core of the current. There was a nice trip to the Azores where the turbulence was found to be relatively strong in the seasonal thermocline, and in layers tens of meters thick, while the Ozmidov scale was only half a meter. Ann Gargett conducted the Fine and Microstructure Experiment (FAME) using our instrument. She showed that dissipation tended to scale with the square of the Vaisala frequency. With the purchase of the Pisces submersible, the Canadians made it available for turbulence measurements. This required modifying the vehicle to remove a dramatic pitch instability as well as designing a framework to mount the probes away from the substantial flow distortion induced by the submersible itself (Osborn and Lueck, 1985).

Based on the results of the Pisces measurements, Stan Wilson of the US Office of Naval Research indicated to Ann Gargett at a meeting of the American Geophysical Union that the research submarine Dolphin could be made available. Instrumenting the submarine was a major undertaking; it was necessary to design an instrument support that did not vibrate at frequencies that would contaminate the shear signals. The frame was made from 10-inch steel pipes and had to be pressurized to withstand test depth of the boat. All pressure cases had to pass Bureau of Ships review to ensure they would not implode, ignite implosion of the mounting frame, and thus threaten the hull.

DIFFUSIVITY FROM DISSIPATION

By the mid 1970s, I was loosing faith in the 1 cgs value for the diffusivity. Both the temperature microstructure measurements and the chemical diffusion experiments were producing lower values. We also had a large amount of dissipation data from different regimes, and the values were smaller than I expected (although I don't really know what I expected).

When thinking about the less-than-expected vertical diffusivity, I wondered if the dissipation measurements could be used to put a limit on the buoyancy flux. Having asked the question in that form, it was only a short step to a production dissipation balance model, with the buoyancy flux estimated from the flux Richardson number times the production. Bob Stewart had often argued that a value of 0.15 was reasonable for the flux Ri. Rex Britter's thesis (which Bob had passed to me with a request to review) was also convincing.

An important consideration to my thinking was that the turbulence in some of the open ocean measurements looked like the shear flow regimes from the Equatorial Undercurrent. Turbulent regions often had a vertical scale substantially exceeding the Ozmidov scale. I concluded they were likely driven by a shear flow, with a vertical scale determining the vertical scale of the patches. This thinking justified the shear production, dissipation, and buoyancy flux model.

CONJECTURES: FINE STRUCTURE – THIN LAYERS – STIRRING – VERTICAL SHEAR – INERTIAL MOTIONS

Carl Eckart's simple separation of stirring and mixing was really very prescient. Quasi horizontal motion drives the stirring and produces the vertical interfaces of large temperature gradients that are often called fine structure. Vertical shear in the lateral motion allows turbulence to extract energy. It is my belief (conjecture) that the shear is of near inertial frequency (Itsweire et al., 1989) but probably not waves since there is no vertical repetition of the thick patches.

While dissipation is important and fortunately quantifiable, it is the stirring processes and their dynamics that need to be understood and somehow quantified. Large scale mapping of dissipation will be of limited use without the understanding of the dynamics of the processes that lead to the dissipation.

APPENDIX

Flow Distortion (see Osborn and Lueck, 1985)

The *Dolphin* submarine was a large body, and we could only locate the probes a limited distance away from the hull. The probes were mounted above the hull to facilitate changing the probes and servicing the electronics. Putting the probes in front of the bow would have required Navy divers to remove the electronics in order to change the probes. In addition, the probes would have been exposed to any surface debris during transit. It would also have lengthened the submarine and made docking extremely difficult. Nobody liked the idea!

Given the proximity of the probes to the hull, it was necessary to consider the effect of the flow distortion. As I recall, it was about 5% increase in the lateral shear and about the same decrease in the vertical. There is also an increase in the axial component of the mean speed. At the time, these were difficult numerical calculations; now, not so much.

Putting the probes on the front of the nose of the submarine would have been problematic because, for structural reasons, they couldn't have been very far from the stagnation point at the bow. The axial speed would have been much reduced and probably, variable due to the stagnation point wandering (Millard et al., 1998; Thorpe et al., 2003).

These problems were brought home when using *Autosub*. The probes were mounted in front of the nose and probably not one full body diameter from the stagnation point. After calculating the effect of the *Autosub* hull, it occurred to me that the pressure case for the electronics probably had an effect and that turned out to be comparable to the effect of the *Autosub* body.

FP07 and Temperature Gradient Spectra

To increase the frequency response of a thermistor, it needs to be small and, hence, is fragile. Originally, Victory Engineering Company was the source for thermistors. When a couple of their engineers left and formed Thermometrics, I asked them about putting the very fine rod thermistor onto the end of a larger and longer glass rod. That was the original FP07, where the thermistor bead was about a quarter inch in front of the larger rod. Slowly, over time, the bead migrated back onto the front edge of the larger rod, no doubt reducing the frequency response. By then, the frequency response didn't matter to me, as I just used the temperature gradient data as a locator for turbulent regions.

As you slow down the speed of the sampling system to increase resolution of the probe, the shear across the sampling platform or the motions associated with the larger turbulent eddies becomes important. The applicability of Taylor's hypothesis becomes problematic.

Temperature gradient spectra plotted on a log-log basis are not "variance preserving" in the sense that equal areas underneath the curve contribute equally to the variance. If both axes are on a linear scale, then the plot is variance preserving. If the abscissa is logarithmic, then the ordinate should be linear but wavenumber times the spectral value. In addition, there needs to be enhancement at higher wavenumber to account for the sensor's spectral response. Hence, log-log plots of uncorrected spectral values against wavenumber are often unconvincing as to whether the variance is fully resolved.

Generally, the vertical axis is also logarithmic to allow for the dynamic range of the signal. That is quite fine as long as the response and factor of wavenumber (to account the logarithmic abscissa) are included.

REFERENCES

Itsweire, E.C., T.R. Osborn, and T.P. Stanton. 1989. Horizontal distribution and characteristics of shear layers in the seasonal thermocline. *Journal of Physical Oceanography* 19:301–320, https://doi.org/10.1175/1520-0485(1989)019<0301:HDACOS>2.0.CO;2.

Millard, N.W., G. Griffiths, G. Finegan, S.D. McPhail, D.T. Meldrum, M. Pebody, J.R. Perrett, P. Stevenson, and A.T. Webb. 1998. Versatile autonomous submersibles—The realising and testing of a practical vehicle. *Underwater Technology* 23:7–17, https://doi.org/10.3723/175605498783259894.

Osborn, T.R., and R.G. Lueck. 1985. Turbulence measurements with a submarine. *Journal of Physical Oceanography* 15(11):1,502–1,520, https://doi.org/10.1175/1520-0485(1985)015<1502:TMWAS>2.0.CO;2.

Thorpe, S.A., T.R. Osborn, J.F.E. Jackson, A.J. Hall, and R.G. Lueck. 2003. Measurements of turbulence in the upper-ocean mixing layer using Autosub. *Journal of Physical Oceanography* 33(1):122–145, https://doi.org/10.1175/1520-0485(2003)033<0122:MOTITU>2.0.CO;2.

ACKNOWLEDGMENTS

At Scripps Institution of Oceanography, Chip Cox, Carl Eckart, and Warren Wooster were kind and very helpful. At the University of British Columbia, my PhD students (David Farmer, Bill Crawford, Rolf Lueck, Ron Ninnis, and Jim Moum) were wonderful. Rolf showed up as an undergraduate, by the time we parted, he was a real friend and colleague. Ann Gargett and Steve Thorpe have been great colleagues and collaborators through the years. George Pickard was a fantastic chairman for the Institute. Bob Stewart's presence shows up both overtly and covertly in so many places. Stan Wilson and Lou Goodman at the Office of Naval Research were crucial contributors to this work.

AUTHOR

Thomas Osborn (osborn@jhu.edu), The Johns Hopkins University, Baltimore, MD, USA.

A Decade of Multi-Month Microstructure Measurements from Seaglider

Luc Rainville, Craig M. Lee, Jason I. Gobat, Geoff B. Shilling, and Ben Jokinen

Over the past 12 years our group has worked to develop a system for collecting extended (many months) dissipation measurements from autonomous platforms. This compact, low-power system has been integrated onto Seaglider with minimal impact on flight and endurance. Microstructure measurements have been acquired over spans as long as six months, but probe failures often occur. Here we describe the system and present statistics for sensor durability computed from deployments over a vast range of conditions and geographical locations.

SEAGLIDER MICROSTRUCTURE SYSTEM

Oceanic turbulence is highly episodic and patchy. Detailed studies with shipbased or rapid profilers have made significant advances linking physical processes and observed turbulence. A different approach, presented here, relies on persistence and long endurance of autonomous platforms to sample across a range of conditions and environments, and to provide access in challenging conditions (e.g. storms, ice-covered environments).

Seagliders are autonomous underwater vehicles that utilize changes in buoyancy, pitch, and roll to move through the water. Seagliders profile between the sea surface and 1,000 m at horizontal (vertical) speeds of roughly 0.25 m s^{-1} (0.1 m s^{-1}), allowing them to transit between waypoints at 20 km day^{-1}. Gliders typically take four to six hours for a 1,000 m dive, which provides a horizontal resolution of 3–5 km. Most Seaglider missions carried out by our team last several months, with endurance exceeding a year under severe energy management. The newest generation of Seaglider, SGX, can operate for about eight to nine months while diving and sampling multiple variables continuously, including microstructure.

To collect sustained measurements of oceanic turbulent dissipation rates while minimizing impact on glider endurance, a fully integrated microstructure system has been developed at the University of Washington Applied Physics Laboratory (APL). The system can accommodate two probes, typically a fast thermistor (FPO7) and a thin-film shear sensor sampling at 400 Hz. Probes and analog signal conditioning boards are provided by Rockland Scientific Inc., integrated into acquisition and processing electronics and software designed and built at APL. The system has been licensed to Rockland Scientific Inc. Careful design for the analog and digital portions of the system results in very low power electronics (~150 mW), in line with the power requirements of other instruments typically integrated on Seagliders.

Microstructure measurements are processed on board to provide near-real-time estimates of dissipation rates, with full-resolution data stored for download after glider recovery. Ensembles are calculated by averaging several overlapping spectra calculated as the data are being acquired. We typically compute a Fast Fourier Transform (FFT) over overlapping blocks of 512 samples using a Tukey window, averaging 18 overlapping blocks (9 independent blocks, 18 degrees of freedom). Effectively, one ensemble is obtained for every vertical meter of profile (10 sec). Particularly for shear, data are despiked and detrended before calculating the FFT, and are masked when the glider's control motors are active. Ensemble spectra are further averaged as 12-point spectra (roughly logarithmic bins) and transmitted at the end of each dive (Rainville et al., 2017). Spectra are scaled and transformed to physical units on the shore-side base station after glider data are processed and forward speed is estimated from the flight model for the entire dive. Dissipation rates are obtained by fitting theoretical spectra (following, for example, Ruddick et al., 2000; Bluteau et al., 2016).

Seagliders sample during both dive and climb, and they are slow enough to resolve the diffusive rolloff at high wavenumbers. Microstructure data from gliders have been shown to be of quality comparable to free-falling instruments (e.g., Wolk et al., 2009; Ferris et al., 2022; and many others in between). Example of Seaglider microstructure data are shown in Rainville et al. (2017).

DURABILITY OF PROBES

Over the last 12 years, our group has conducted many deployments of the microstructure system, in environments ranging from the equator to the Arctic (Table 1). The vast majority of these deployments were supported by the Office of Naval Research. Overall, through summer of 2023, we have collected 13,536 profiles of temperature microstructure (totaling 2,008 days of sampling), and 6,780 profiles of shear microstructure (1,298 days of sampling).

TABLE 1. List of Seagliders with microstructure sensors, deployed by the Integrative Observational Platforms group, University of Washington. Note that the duration listed is for the mission, not the duration of good microstructure data. Deployments with other energy-expensive sensors. ADCP = a Nortek Signature 1000 Acoustic Doppler current profiler. PMAR = Passive Marine Acoustic Recorder, developed at the University of Washington Applied Physics Laboratory.

YEAR(S)	DEPLOYMENT	DATES	NUMBER OF GLIDERS	DURATION	OTHER SENSORS
2010	ITOP (Taiwan)	Sep 2010	3 gliders	3 months	
2011	OKMC (Taiwan)	Jun 2011	1 glider	1 month	
2012–2013	SPURS-1 (North Atlantic)	Sep 2012 to Mar 2013	3 gliders	6 months	
		Mar 2013 to Aug 2013	3 gliders	6 months	
2013	NABOS (Eastern Arctic)	Aug 2017 to Oct 2017	1 glider	2 months	
2014	MIZ (Western Arctic)	Aug 2017 to Oct 2017	4 gliders	3 months	
2016–2017	SPURS-2 (Equatorial Pacific)	Aug 2016 to April 2017	3 gliders	7 months	PMAR
		Aug 2017 to Oct 2017	2 gliders	3 months	PMAR
2018–2020	NISKINE (North Atlantic)	May 2018 to Oct 2018	1 glider	5 months	ADCP
		Jun 2019 to Aug 2019	1 glider	2.5 months	ADCP
		Oct 2019 to Apr 2020	2 gliders	5 and 6 months	ADCP
2019	MISOBOB (Bay of Bengal)	Jul 2019 to Jan 2020	2 gliders	7 months	PMAR
2019–2020	Guam Salinity (Pacific)	Oct 2019 to Jan 2020	2 gliders	3 months	PMAR and ADCP
2021	NORSE (Nordic Seas)	Sep 2021	2 gliders	1 month	PMAR and ADCP + Wave Glider
2022	ARCTERX (Pacific, near Guam)	Mar 2022 to Apr 2022	1 glider	2 months	PMAR and ADCP + Wave Glider

Microstructure probes are notoriously delicate. The glass bead at the tip of an FPO7 fast thermistor will break if touched, even gently. Despite this, probe survivability on most missions ranged from days to months, though a few probes failed on deployment. Every mission has its own story, and there are numerous possible failure modes for these systems, but the aggregate statistics produced by considering this large collection of deployments provides a valuable perspective on probe durability.

Overall, the temperature microstructure system sampled for the entire mission for 18 out of 41 deployments (44%, Figures 1a and 2a) and 8 out of 26 deployments for shear microstructure (31%, Figures 1b and 2b). Probe failure, often associated with collisions, is the root cause of nearly all microstructure system failures. More careful analysis of the failure modes (progressive, catastrophic, etc.) is underway. Here we report the length of time (Figure 1) and the number of profiles (Figure 2) of successfully recorded microstructure.

Because missions do not all have the same duration, it is helpful to compare the probability density function of the number of days of successful microstructure sampling, in black, with mission duration, in gray in Figure 1c,d. While some microstructure data sets extend to 200 days or more, about than 50% last less than 25 days. While 40% of the missions lasted more than 120 days, only 10% of the temperature microstructure time series lasted that long (5% for shear).

For several missions the microstructure system was sampling only during the dive or climb portion of the glider profiles, so the number of microstructure profiles of sometimes smaller than the number of profiles in the mission (Figure 2b). We include the statistics in terms of number of profiles for completeness, to provide our results in terms of pressure cycles, which might contribute to probe failure.

Overall, the microstructure system on Seaglider is robust and allow to collect long term turbulence observations in remote and challenging environments. Several thousands of profiles have been collected. A fairly high rate of failure should be expected due to the delicate nature of the sensors.

REFERENCES

Bluteau, C.E., N.L. Jones, and G.N. Ivey. 2016. Estimating turbulent dissipation from microstructure shear measurements using maximum likelihood spectral fitting over the inertial and viscous subranges. *Journal of Atmospheric and Oceanic Technology* 33(4):713–722, https://doi.org/10.1175/JTECH-D-15-0218.1.

Ferris, L., D. Gong, C.A. Clayson, S. Merrifield, E.L. Shroyer, M. Smith, and L. St. Laurent. 2022. Shear turbulence in the high-wind southern ocean using direct measurements. *Journal of Physical Oceanography* 52(10):2,325–2,341, https://doi.org/10.1175/JPO-D-21-0015.1.

Rainville, L., J. Gobat, C. Lee, and G. Shilling. 2017. Multi-month dissipation estimates using microstructure from autonomous underwater gliders. *Oceanography* 30(2):49–50, https://doi.org/10.5670/oceanog.2017.219.

Ruddick, B., A. Anis, and K. Thompson. 2000. Maximum likelihood spectral fitting: The Batchelor spectrum. *Journal of Atmospheric and Oceanic Technology* 17(11):1,541–1,555, https://doi.org/10.1175/1520-0426(2000)017<1541:MLSFTB>2.0.CO;2.

Wolk, F., R. Lueck, and L. St. Laurent. 2009. Turbulence measurements from a glider. Pp. 26–29 in *OCEANS 2009*, MTS/IEEE Biloxi - Marine Technology for Our Future: Global and Local Challenges, October 26–29, 2019, Biloxi, Mississippi, https://doi.org/10.23919/OCEANS.2009.5422413.

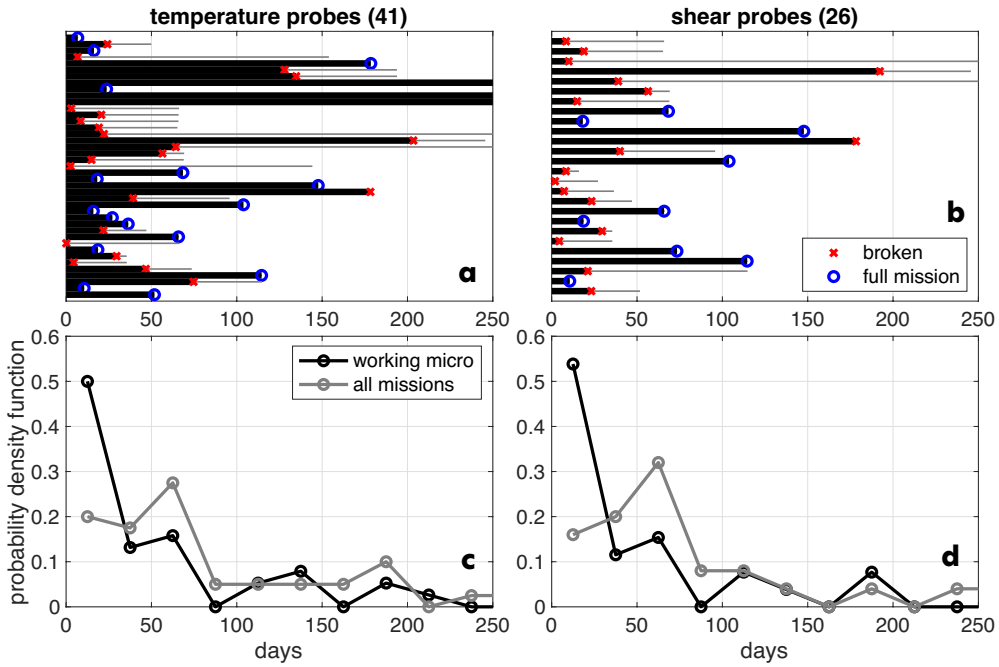

FIGURE 1. Microstructure probe durability in terms of time (days), for (a) microtemperature and (b) shear. The black bars in panels a and b indicate the number of days the microstructure probe was working correctly. The gray lines are the total number of days of each mission. Missions when the probe was still working at recovery are in blue, and in red if it failed during the mission. (c,d) Probability density functions for total mission (gray), and duration of microstructure time series (black).

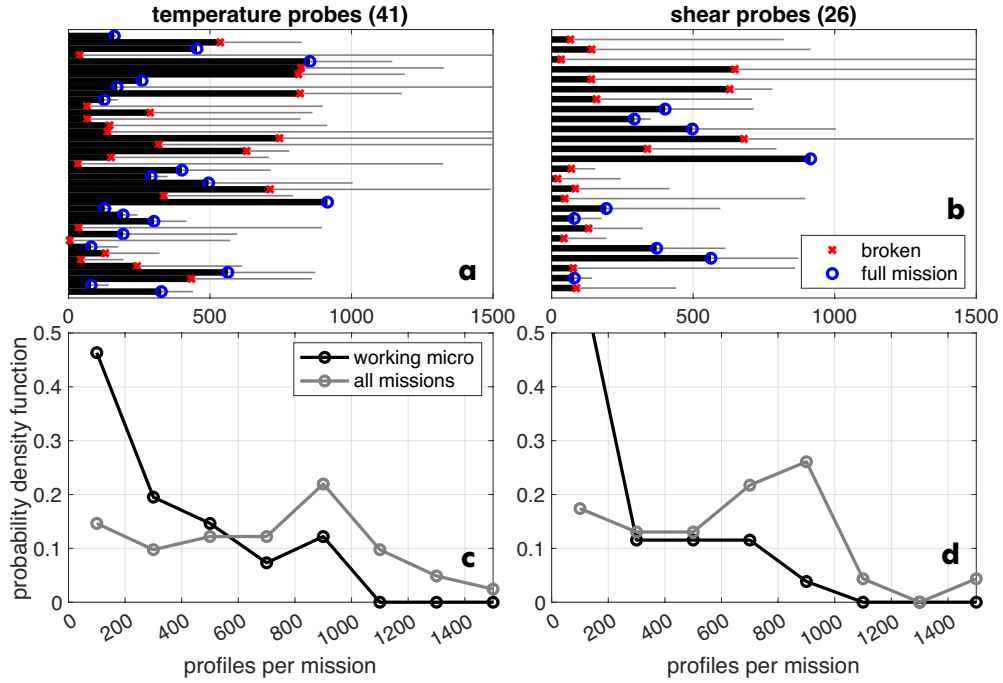

FIGURE 2. Same as Figure 1, but microstructure probe durability in terms of number of profiles.

ACKNOWLEDGMENTS

We are grateful for the support from the Office of Naval Research throughout the years, which allowed us to develop and continuously improve the integration of microstructure on Seagliders. We would like to acknowledge contributions from Neil Bogue, Rolf Lueck, Fabian Wolk, Jim Bennett, and many others for fruitful discussions about the platform, and the analog and digital components of the Seaglider microstructure system.

AUTHORS

Luc Rainville (lucrain@uw.edu), **Craig M. Lee**, **Jason I. Gobat**, **Geoff B. Shilling**, and **Ben Jokinen**, all at Integrative Observational Platforms Group (https://iop.apl.uw.edu/), Applied Physics Laboratory, University of Washington, Seattle, WA, USA.

Near-Real-Time Processing and Telemetry of Measured Turbulent Dissipation Rates by Autonomous Underwater Gliders

Justin Shapiro, Laur Ferris, and Louis St. Laurent

Autonomous underwater vehicles are an established platform for conducting direct microstructure measurements of turbulent kinetic energy (TKE) dissipation rate (ε). This technique requires measuring the velocity shear ($\partial u/\partial z$) at a high sampling rate (~512 Hz), which generates raw data at a rate of 100–400 MB per day. Even drastic decimation and compression of the raw data would still result in files orders of magnitude greater than the transmission capacity of available satellite communication options which have low bandwidth (~250 bytes per second). Historically, an operator could only process raw data into turbulent dissipation rate estimates, ε, after vehicle recovery, carrying a risk of total data set loss if the glider was lost at sea, as well as opportunity cost for adaptive sampling (using turbulence data to inform piloting or ship operations). We solve this problem by equipping Slocum G2 gliders with a low-power, embedded computer to conduct in situ data processing and near-real-time telemetry of ε. An example of data from the recent ONR NISKINE field program is presented.

TURBULENCE PROCESSING (TP) SYSTEM: OVERVIEW OF ELECTRONIC COMPONENTS

The turbulence processing glider system consists of a Slocum G2 glider (Figure 1a) outfitted internally with a turbulence processor (TP, an Embedded ARM TS-4900 computer with 1GHz i.MX6 and 2GB RAM), and externally with a Rockland Scientific MicroRider. The TP consumes 0.5–3.4 W when active and otherwise consumes microwatts in deep sleep. Both the computer and the MicroRider are powered and commanded from the glider's payload bay using the commercial off-the-shelf cable penetration configuration (Figure 1b). The three relevant subsystems (the factory-included vehicle science controller, the MicroRider, and the TP) are connected using a custom-built wiring harness and circuitry enabling serial communication between any of these devices. The science computer and the TP have two independent channels of communication: a serial console channel (which enables remote debugging and reconfiguration of the TP while the glider is deployed) and a command interface (which is explicitly used for sensor automation). In addition to a serial connection, the TP is also connected to the MicroRider via a USB interface, enabling higher-bandwidth transfer of data files from the MicroRider to the TP. The MicroRider wiring was modified from its factory configuration to feed the USB and serial MicroRider channels into the glider's hull through a single MCBH8 underwater connector (Figure 1b).

Our gliders' missions are typically configured to sample microstructure during the climb phase of the trajectory, enabling acquisition of accurate velocity shear measurements through the surface boundary layer up to the air-sea interface. TP gliders manage processing in a delayed real-time sense, leveraging the dive immediately following acquisition of each microstructure profile for data transfer from the MicroRider to the TP, processing of dissipation rate on the TP, and transfer of that dissipation rate profile from the TP to the glider. MicroRider and TP operation are configured as a standard oceanographic sensor in the Slocum glider's mission and mission acquisition (MA)

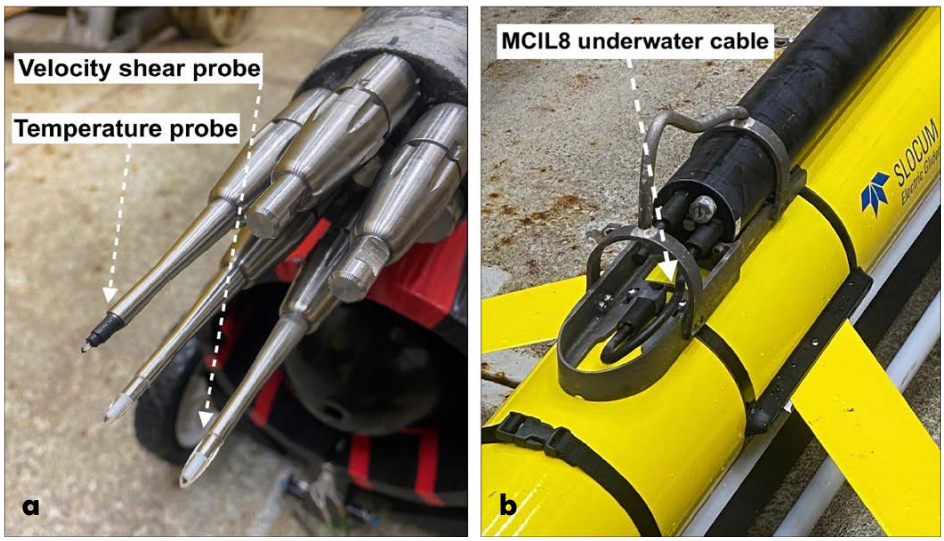

FIGURE 1. (a) MicroRider temperature and velocity shear probes. (b) USB and serial MicroRider channels feed through the glider's hull using a single MCIL8 underwater cable.

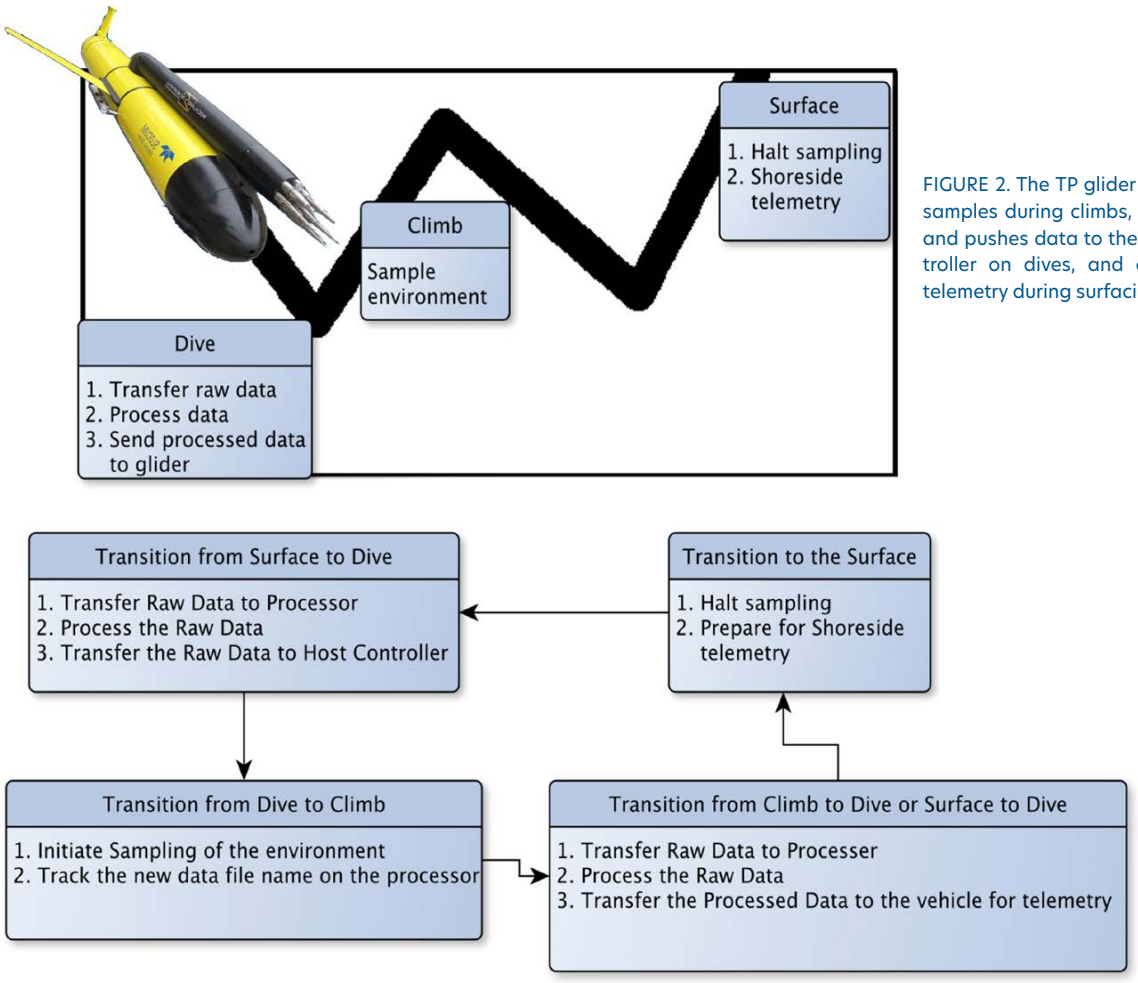

FIGURE 2. The TP glider nominally samples during climbs, processes and pushes data to the host controller on dives, and completes telemetry during surfacing events.

files. The turbulence processing system drives TP behavior based on whether the TP/MicroRider system should be activated for a particular dive phase and whether the glider is diving or climbing (determined from its pressure sensor). Figure 2 schematically represents the sequence of events and is described as follows:

1. The glider senses it has begun to initiate a climb and activates the TP driver as per MA file configuration. The TP driver waits for the dive to stabilize. The glider's vehicle science controller wakes the TP and commands the TP into sampling mode. The TP initiates the MicroRider's data acquisition and then puts itself into low-power sleep.
2. The glider's vehicle science controller tells the MicroRider to suspend sensing. This prompts the MicroRider to cease data acquisition, flush all data to log files (called .P files), and power off.
3. The glider initiates a dive and activates the TP driver as per MA file configuration. The TP driver waits for the dive to stabilize, then wakes the TP, commands it into processing mode, and powers on the MicroRider. The TP downloads the most recently acquired .P file (containing one microstructure profile) via USB, and then commands the vehicle science controller to remove power from the MicroRider. The TP begins processing the .P file while the vehicle science controller awaits data lines containing a time series of the processed variables (including ε) and a checksum to validate each line of the data transfer.

The key parameter used to quantify turbulence is TKE dissipation rate (ε, [W kg^{-1}]), which quantifies the rate at which the kinetic energy of microscale motion is lost to molecular viscosity. Glider vibrations (and, by extension, the rigidly attached velocity shear probes) can produce false shear variance in the same wavenumber and frequency range as true turbulence. To decontaminate the observed velocity shear spectra, MicroRiders are equipped with either multiaxis analog accelerometers or a pair of one-dimensional vibration sensors mounted parallel to the shear probes. These vibration estimates enable deconvolution of vibration spectra from measured shear spectra (Goodman et al., 2006). Dissipation rate (ε) is estimated from the decontaminated shear spectra using the procedure long used for vertical microstructure profiles, as detailed in Gregg (1999). Discussion of methodology specific to glider-based microstructure is given by Fer et al. (2014), Palmer et al. (2015), and St. Laurent and Merrifield (2017). Spectra are examined using a 2048-element window over which a 1024-element fast Fourier transform (FFT) is applied.

Adjacent 1024-element bins are treated using a Hanning window with 50% overlap. For a nominal glider speed of 25–30 cm s^{-1}, this methodology produces one spectral variance estimate per ℓ = 0.5 – 0.6 m of along-trajectory path. This analysis results in pseudo vertical profiles with dissipation rate estimates reported at 25–30 cm increments in depth. The limits of integration are taken from approximately 1 cpm (cycle per meter) to an upper wavenumber of either 100 cpm or, more frequently, the wavenumber demarcating the transition from the resolved dissipative subrange to the range dominated by electronic noise (identified using a 5th order polynomial fit of the decontaminated spectra). Spectra that deviate significantly from the canonical Nasmyth spectrum are not included in dissipation estimates. This methodology is sensitive to dissipation rate estimates as low as 5 x 10^{-11} W kg^{-1} (Wolk et al., 2009).

Estimates of ε are sent from the TP to the vehicle science controller in CSV format, which includes an acquisition timestamp, slow-rate pressure measured by the MicroRider, and an independent ε estimate for each shear probe (a treatment resilient to the event in which one shear probe malfunctions due to biofouling or plastic deformation due to repeated pressurization and depressurization during flight). All values are valid for the center of the Hanning window. Because satellite telemetry from gliders is heavily bandwidth-limited, a data budget was enforced to prevent excessive transmission times. In the event that more than 312 lines of data (or ~20 kB, an issue for profiles over 250 m at a nominal vertical velocity of 30 cm s^{-1}), are generated from a single profile, the ε time series is evenly decimated to write 312 lines of data to the CSV. The dissipation estimates are pushed from the CSV to the glider line by line for storage in the Slocum glider's native .TBD/.EBD format and are available for telemetry to shore when the vehicle reaches the surface. In either case, full resolution, processed data are stored on the TP, and raw MicroRider .P files are stored on both the TP and on the MicroRider.

FIRST LONG DURATION TRIAL: DEPLOYMENT IN THE ICELANDIC BASIN

The first open-ocean sea trial of the system was conducted in April–June 2019 southwest of Iceland as a part of the Office of Naval Research (ONR) Near Inertial Shear and Kinetic Energy in the North Atlantic Experiment (NISKINE) Departmental Research Initiative. A vessel of opportunity, Icelandic ice tug M/V *Togarinn*, deployed eight autonomous assets to complete a general survey mission preceding a process cruise in May–June 2019. The vehicles were deployed in a subsea canyon outside the Icelandic exclusive economic zone and flown southward in a coordinated fashion toward the intensive observation area for the process cruise. The deployed assets included (1) the Slocum glider *Apollo* equipped with a TP, and (2) a Liquid Robotics Wave Glider SV3 equipped with sensors that can measure surface-forcing wind speed and direction, and wave amplitude and direction, as well as a 100 m ADCP. While both systems were used in parallel during the study, data from the SV3 will not be discussed here.

The complementary payloads of *Apollo* and the SV3 would enable the measurements of upper ocean turbulence and surface meteorological forcing, both undisturbed by large vessel or buoy effects. The systems demonstrated consistent performance throughout the two-month sea trial, sampling continuously over the Reykjanes Ridge.

When piloting a glider, there is a trade-off between the depth of the profiles and the spatial sampling resolution (shallower profiles allow high horizontal resolution). For the 2019 NISKINE deployment, near-real-time turbulence data (Figure 3) were used to optimize *Apollo*'s sampling strategy. For the first several weeks of the survey, the glider followed a shallow (0–350 m) sampling pattern during periods of active surface forcing as measured by the Wave Glider and then transitioned to an adaptive sampling pattern on May 18. After around May 18, surface forcing weakened, and the vehicle crossed over the Reykjanes Ridge, providing a period when the vehicle could explore more of the water column. At this point, the glider concentrated on capturing profiles of the evolution of actively mixing layers (AMLs) during storm events and dove to 1,000 m after these events subsided. Two such example are on May 19 and June 4, when the glider was switched to collected deep profiles after the AML had retracted following May 13 and May 31 storm events. In addition to capturing the rapid evolution of the surface mixing layer in response to shear-convective turbulence forced by the storms, the adaptive sampling pattern captured a deep scattering layer (Figure 3, 100–250 m) and bottom-enhanced turbulence (Figure 3, 600–1,000 m), likely driven by flow-topography interaction with the Reykjanes Ridge.

More recently, we operated additional Slocum gliders with TP systems during the ONR Island Arc Turbulent Eddy Regional Exchange (ARCTERX) and Northern Ocean Rapid Surface Evolution (NORSE) programs. Publications describing these studies will be forthcoming. We plan to develop onboard self-tuning of the glider flight model by matching the dissipation statistics of the up-and-down trajectories to account for angle-of-attack variations, as we currently do in post-mission analysis. We further plan to implement a newer version of the TP to work with the G3 Slocum variants, employing the new G3 "payload computer" to handle interaction between the TP and the glider's science and flight computers. This will supersede the use of customized glider source code currently in use on the G2 that enables support of the TP.

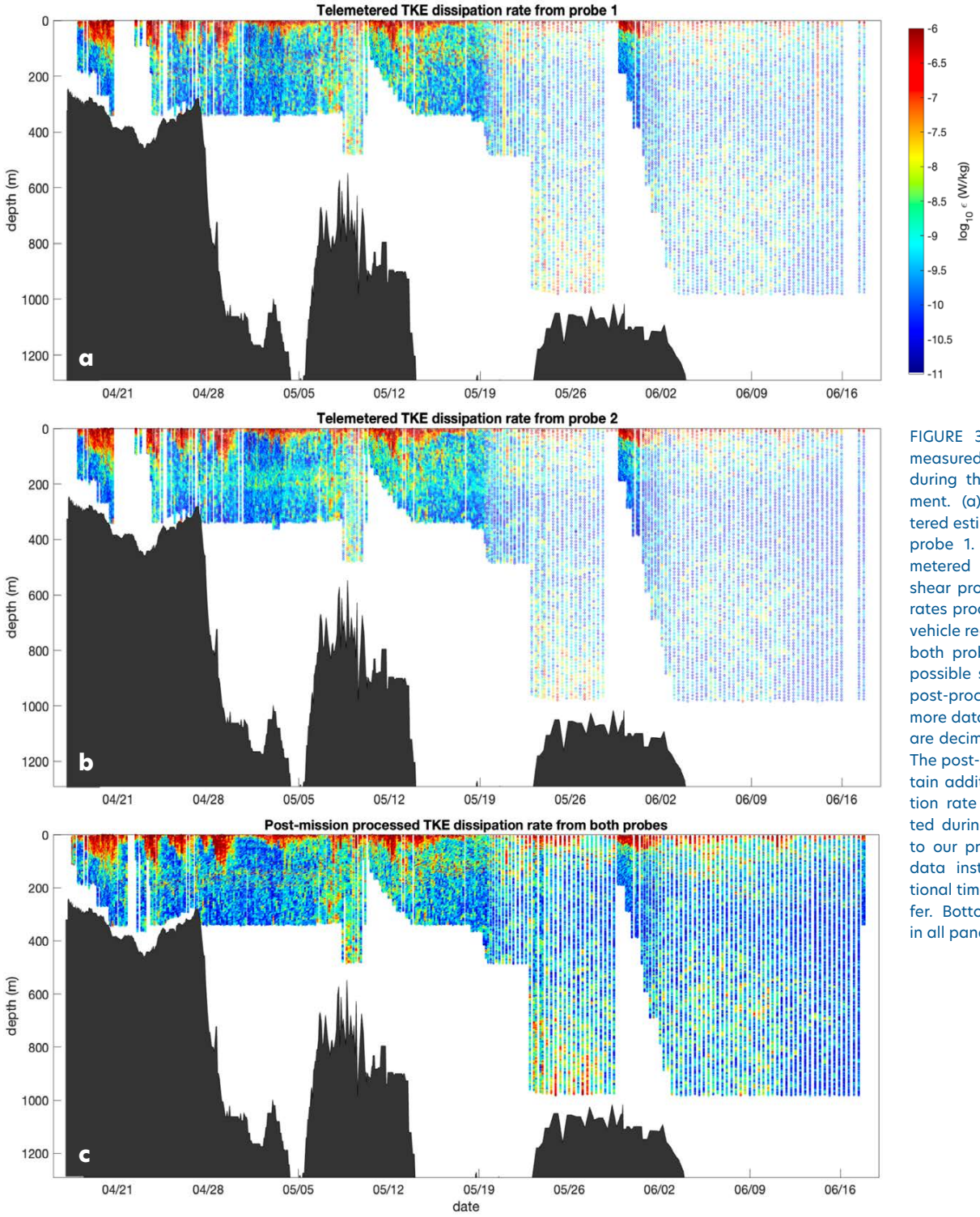

FIGURE 3. TKE dissipation rates measured by TP glider *Apollo* during the 2019 NISKINE deployment. (a) Near-real-time telemetered estimates from velocity shear probe 1. (b) Near-real-time telemetered estimates from velocity shear probe 2. (c) TKE dissipation rates processed post-mission after vehicle recovery, using signals from both probes to produce the best possible single estimate of ε. The post-processed data contain vastly more data, as the telemetered files are decimated to reduce their size. The post-processed data also contain additional profiles of dissipation rate that were not transmitted during the glider mission due to our preference to collect more data instead of spending additional time at surface for file transfer. Bottom bathymetry is shown in all panels.

REFERENCES

Fer, I., A.K. Peterson, and J.E. Ullgren. 2014. Microstructure measurements from an underwater glider in the turbulent Faroe Bank Channel overflow. *Journal of Atmospheric and Oceanic Technology* 31(5):1,128–1,150, https://doi.org/10.1175/JTECH-D-13-00221.1.

Goodman, L., E.R. Levine, and R.G. Lueck. 2006. On measuring the terms of the turbulent kinetic energy budget from an AUV. *Journal of Atmospheric and Oceanic Technology* 23(7):977–990, https://doi.org/10.1175/JTECH1889.1.

Gregg, M.C. 1999. Uncertainties and limitations in measuring ε and χ_T. *Journal of Atmospheric and Oceanic Technology* 16(11):1,483–1,490, https://doi.org/10.1175/1520-0426(1999)016<1483:UALIMA>2.0.CO;2.

Palmer, M., G.R. Stephenson, M.E. Inall, C. Balfour, A. Dusterhus, and J.A.M. Green. 2015. Turbulence and mixing by internal waves in the Celtic Sea determined from ocean glider microstructure measurements. *Journal of Marine Systems* 144:57–69, https://doi.org/10.1016/j.jmarsys.2014.11.005.

St. Laurent, L., and S. Merrifield. 2017. Measurements of near-surface turbulence and mixing from autonomous ocean gliders. *Oceanography* 30(2):116–125, https://doi.org/10.5670/oceanog.2017.231.

AUTHORS

Justin Shapiro (jshapiro@apl.uw.edu), **Laur Ferris**, and **Louis St. Laurent**, all at the Applied Physics Laboratory, University of Washington, Seattle, WA, USA.

Autonomous Turbulence Profiling with the microALTO Float

Fritz Stahr, Rolf G. Lueck, and Steven R. Jayne

We describe the development of a profiling float equipped with turbulence sensors. The turbulence data are processed on board the float, and the spectra are returned by satellite communication.

A COLLABORATION OF COMPANIES

Profiling floats offer an expendable, low-noise platform from which to make turbulence measurements, free from the vibrations introduced by propellers or tethers. Rockland Scientific International Ltd. (RSI) and MRV Systems LLC (MRV) worked together to create a 2,000 m capable float, the microALTO, which carries two Rockland turbulence probes and associated electronics in addition to a standard RBR Ltd CTD sensor system for ocean profiling. The Rockland turbulence sensors are the modern versions of the micro-temperature probes originally created by Osborn and Cox (1972) and velocity shear probes (Osborn, 1974). This collaboration led to designing and completing three prototypes through 2020 and 2021, with field trials in December 2021 before shipping two to the first customer in early 2022.

SYSTEM DESCRIPTION

The microALTO consists of an MRV ALTO profiling float with an RBR CTD (Halverson et al., 2020; Nezlin et al., 2020) on top along with two carefully positioned Rockland probe holders for holding either FP07 temperature probes and/or velocity shear probes (Osborn and Crawford, 1980) patterned after their successful original equipment manufacturer product the microPod (Figure 1). This new system is known as the MAPLe, and a block diagram is shown in Figure 2. In addition to the float's normal electronics (CPU, Iridium SBD modem, GPS, etc.), the microALTO contains a special power-supply board to provide ultraquiet voltage to the MAPLe system and special float-control code for commands and file transfers to shore. That special control code allows the float operator to choose which MAPLe configuration file is used by that system to collect turbulence data on each dive by sending specific filename pointers via the Iridium communications system. It also provides a satellite path for the MAPLe system to return processed files to shore that contain multi-point spectra for each probe on the float (see Figure 3 for an example).

FIELD TRIALS AND DATA

Two particular Rockland sensor combinations were tested in Puget Sound, Washington, in order to validate the functionality of the whole system and provide input for system improvements. One float was outfitted with two FP07 temperature probes (TT) and the other with one FP07 and one shear probe (TS). The field trials were over three days in December 2021, with typical wintertime fjord-type estuary mixing processes underway.

Three key aspects were evaluated in a series of about five to six dives per day: systematic noise generation, data recovery, and piloting for the most effective turbulent data collection. This showed that the pump motor on the float induces noise in the shear spectra but not in the temperature spectra. This is similar to prior experience with other platforms such as gliders (Wolk et al., 2009), where vibration of the body create a spurious shear signal (Wolk et al., 2002). It was also found that the "ice bumper" on the antenna introduced a false peak in the shear spectra. Based on these results, no microALTO will include anything on top of the antenna to protect it or the sensors. In addition, the returned "motor log file" is critical for processing the full data files recovered from the float, and that achieving vertical ascent speeds of 20 cm s^{-1} is possible but requires significant pump time near the dive apogee in a manner that minimizes further pumping during the float ascent phase when the MAPLe system is running with shear probes. One other new feature from Rockland was tested: a mechanical probe-tip protector for the FP07 microtemperature probe. That was also successful in terms of not having any influence on the temperature spectra observed. This field trial demonstrated that data from 200 m long turbulence profiles comes back in a reasonable amount of surface time.

FIGURE 1. The microALTO float showing the RBR CTD (red unit on top right) and antenna (top middle) alongside the Rockland Scientific MAPLe microstructure turbulence probe kit (top left). *Image from https://www.mrvsys.com/products/microalto*

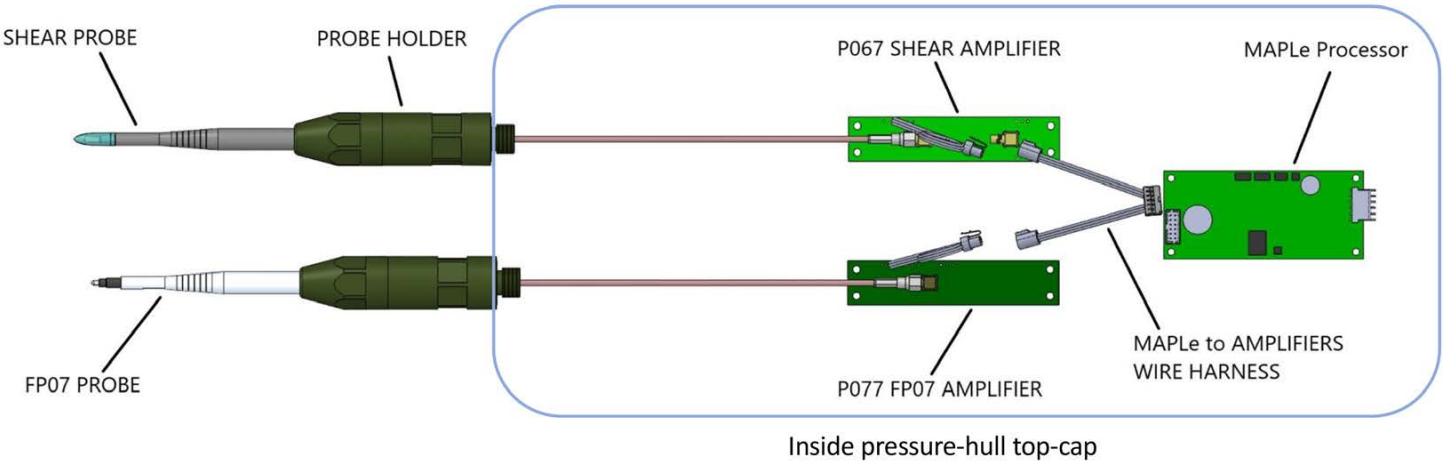

FIGURE 2. Diagram of Rockland Scientific's MAPLe system in the microALTO float.

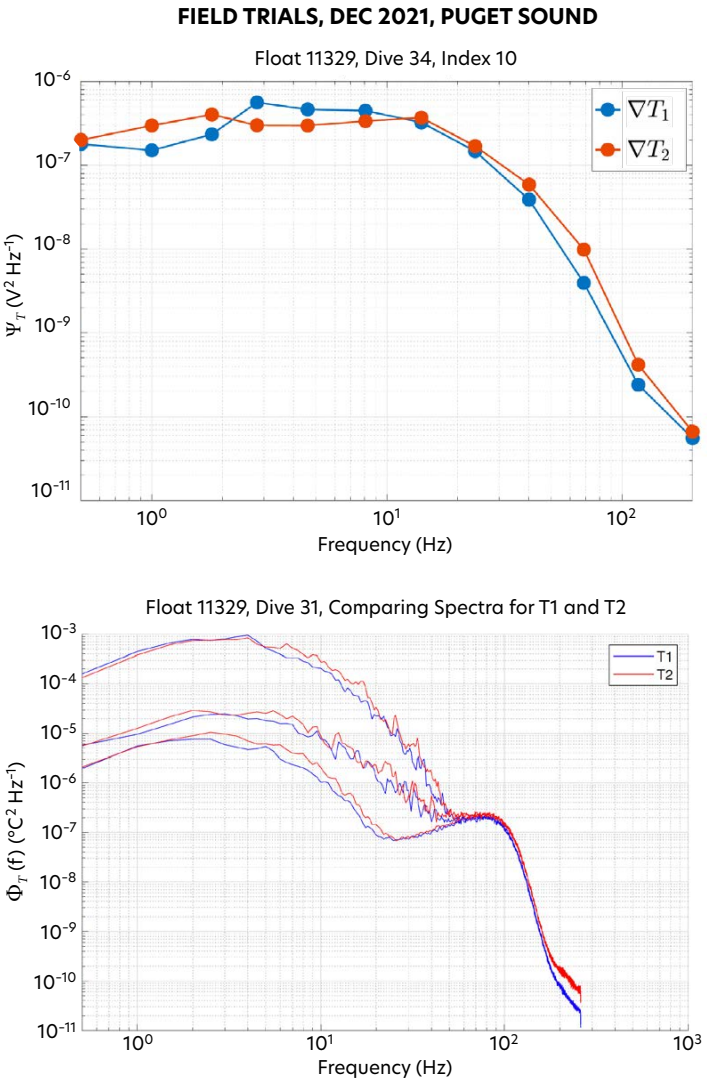

FIGURE 3. Example of data returned from a MAPLe system in a microALTO float. The top panel shows data as processed on board the float and returned by Iridium satellites from the float. The bottom panel shows similar data, but after downloading the full data file post-recovery of the float.

SUMMARY

The microALTO profiling float, equipped with turbulence sensors for either, or both, temperature and shear, has been developed and tested in field trials. It is being offered to customers worldwide by MRV Systems. The choice of Rockland sensor combination needs to be specified by the customer in advance of float fabrication due to the distinct amplifiers for the different probe types that are installed inside each float as part of the RSI MAPLe system. The first microALTOs were used in the western Pacific in July–August 2022.

REFERENCES

Halverson, M., E. Siegel, and G. Johnson. 2020. Inductive-conductivity cell. *Sea Technology* 61(2):24–27.

Nezlin, N.P., M. Dever, M. Halverson, J.-M. Leconte, G. Maze, C. Richards, I. Shkvorets, R. Zhang, and G. Johnson. 2020. Accuracy and long-term stability assessment of inductive conductivity cell measurements on Argo floats. *Journal of Atmospheric and Oceanic Technology* 37:2,209–2,223, https://doi.org/10.1175/JTECH-D-20-0058.1.

Osborn, T.R. 1974. Vertical profiling of velocity microstructure. *Journal of Physical Oceanography* 4:109–115, https://doi.org/10.1175/1520-0485(1974)004<0109:VPOVM>2.0.CO;2.

Osborn, T.R., and C.S. Cox. 1972. Oceanic fine structure. *Geophysical Fluid Dynamics* 3:321–345, https://doi.org/10.1080/03091927208236085.

Osborn, T.R., and W.R. Crawford. 1980. An airfoil probe for measuring turbulent velocity fluctuations in water. Pp. 369–386 in *Air-Sea Interaction: Instruments and Methods*. F. Dobson, L. Hasse, and R. Davis, eds, Plenum, https://doi.org/10.1007/978-1-4615-9182-5_20.

Wolk, F., R.G. Lueck, and L. St. Laurent. 2009. Turbulence measurements from a glider. In *OCEANS 2009,* Conference held October 26–29, 2009, Biloxi, Mississippi, https://doi.org/10.23919/OCEANS.2009.5422413.

Wolk, F., H. Yamazaki, L. Seuront, and R. Lueck. 2002. A new free-fall profiler for measuring biophysical microstructure. *Journal of Atmospheric and Oceanic Technology* 19:780–793, https://doi.org/10.1175/1520-0426(2002)019<0780:ANFFPF>2.0.CO;2.

AUTHORS

Fritz Stahr (stahr@uw.edu), MRV Systems, Seattle, WA, USA. **Rolf G. Lueck**, Rockland Scientific International, Victoria, BC, Canada. **Steven R. Jayne**, Woods Hole Oceanographic Institution, Woods Hole, MA, USA.